Low Temperature Volume Expansion of LiH:LiT

by

Theodore Anthony Dellin

A dissertation submitted to the Graduate Faculty in Physics in partial fulfillment of the requirements for the degree of Doctor of Philosophy, The City University of New York.

1969

This manuscript has been read and accepted by the Graduate Faculty in Physics in satisfaction of the dissertation requirement for the degree of Doctor of Philosophy.

6/22/69
date

Robert D. Hatcher
Chairman of Examining Committee

6/23/69
date

Executive Officer

DR. C. R. FISCHER

DR. B. KRAMER

DR. F. MARTINO

DR. R. SMOLUCHOWSKI
Supervisory Committee

The City University of New York

To my wife, Arlene, without whose constant understanding and devotion this study would not have been possible.

Foreward

I would like to express my deep appreciation to Drs. Robert Hatcher and C. Rutherford Fischer who directed this study. Their comments pertaining to the statement of the problem, guidance, and criticism were extremely valuable. In addition, I would like to thank Dr. George Dienes for his comments on this work and for providing me with the opportunity to work at Brookhaven National Laboratory where this study was performed.

Table of Contents

List of Tables

List of Tables

List of Figures

I. Introduction

The production of defects in crystals exposed to external radiation has been studied for many substances.[1,2] Crystals of LiH experience self damage when some of the H^- ions are replaced by their isotope T. The T^- ions undergo β decay into He^o atoms:

$$T^- \longrightarrow He^o + e^- \qquad (1)$$

The T^- has a half life of 12.4 years and the β particles have a maximum energy of 18 keV and an average energy of 5.6 keV.

Pretzel, Vier, Szklarz, and Lewis[3] found that at temperatures below 0 ^oC (the low temperature region) LiH crystals containing several percent LiT expand by about 5 percent in 1000 days. The expansion is linear in the dose rate. In heavily damaged samples they found NMR signals that indicated the presence of metallic lithium, but not of hydrogen gas. They observed the ESR signals of the body center cubic form of metallic lithium if the damaged samples are heated to room temperature. They discovered that the volume expansion was proportional to the growth of an optical absorption band at 5400 $\AA$ and a paramagnetic center. They interpret the volume expansion by assuming that when the T^- decays into He^o, the He^o moves into an interstitial position and the resulting vacancy eventually captures the electron of the β decay to form an F center.

Their results for the high temperature region (from 23 to 400 °C) are more complicated. The volume expansion undergoes a rapid first stage followed by a lesser second growth stage. As the temperature increases the volume expansion increases and at 400 °C amounts to over 80 percent growth in 200 days. In this high temperature range several types of aggregations have been observed: 1) small particles of metallic lithium precipitate; 2) bubbles of He and H_2^* (hydrogen gas and its isotopes) form; and 3) cavities. The expansion plus these other effects often cause the crystals to fracture.

Pretzel and Petty[4] working at -196 °C and using X-ray diffraction, found no change in the lattice parameter of LiH upon irradiation by external tritium β particles for 100 days. Alkali halides exposed under the same conditions showed a considerable increase in lattice parameter. They attribute the growth in the alkali halides to the formation of Frenkel pairs in the negative ion sublattice.

Jones et al[5] studied the high temperature volume expansion of LiT, LiTD, and $LiTD_2$. The expansion of LiH with 40 percent LiT observed by Pretzel et al falls between the expansion of LiTD (50 percent T^-) and $LiTD_2$ (33 percent T^-) observed by Jones et al at the same temperature. They have fit their high temperature volume expansion to the form:

$$V(t) = V_{\infty} (1 - \exp(- d\ t)) \qquad (2)$$

where V(t) is the percent volume increase at a time, t, V_{∞} is the final percent volume increase, and d is a constant. Pretzel's more comprehensive volume expansion data do not fit this form.

Souers, Jolly, and Cline[6] found that the volume growth of LiH containing 40 mole percent LiT was proportional to the amount of $H_2^{\#}$ and metallic lithium produced in the first stage growth for temperature from 23 to 250 °C. They propose that the second stage growth is due to the He°.

It is the main intent of this study to suggest a possible mechanism to explain the low temperature volume expansion of LiH:LiT crystals. In Section II interactions between constitutent ions and atoms that were used in the calculations are presented; in III the method of defect calculations is described; in IV the results of twenty-four defect calculations are presented; in V the mechanism for radiation damage is proposed; and in VI a summary of the results is given.

II. Quantum Mechanical Interactions

For the calculations of defect properties that are discussed in IV two body repulsive interactions between the host ions, i.e. $Li^{+}-H^{-}$, $H^{-}-H^{-}$, and $Li^{+}-Li^{+}$ are needed. For defects involving foreign atoms the additional interactions between the foreign atoms and the host ions, i.e. $He^{o}-H^{-}$ and $He^{o}-Li^{+}$, are required.

Empirical functions for the repulsive interactions in LiH have been investigated by Varshni and Shulka.[7] Their use in defect calculations has several drawbacks. The experimental evidence used to determine crystal interactions: cohesive energy, lattice parameter, compressibility etc., provides information for interactions in only a small region around the equillibrium internuclear separation. Thus there is an uncertainity about the functional form of the repulsion since several forms can fit the data reasonably well. In addition, in defect calculations the ions surrounding defects move considerably offsite. Therefore, the interactions would have to be extrapolated beyond the range of the data. Finally, to study the radiation damage of LiH:LiT defects involving foreign atoms have to be considered. With empirical interactions for the host ions, a separate method would have to be developed to obtain the interactions with the foreign atoms.

Fischer, Dellin, Harrison, Hatcher, and Wilson[8] have

determined quantum mechanical two body interactions for LiH suitable for defect calculations. They used determinantal wave functions made up of various one electron functions. Using determinants made up of screened hydrogenic wave functions, $\Psi \sim \exp(-\delta r)$, they calculated the cohesive energy, lattice parameter, and compressibility for various values of the screening parameter, δ, of the negative hydrogen ion.

The interactions corresponding to a hydrogen screening parameter of .9 (in atomic units) were used in this work. This is a considerably more contracted hydrogen ion than the free ion which has a screening parameter of .6875. The value of the cohesive energy predicted by this model is -9.69 eV per ion pair. Anderson[9] determined the experimental value of -9.44 eV per ion pair. The lattice constant is 2.216 Å compared with the experimental value of 2.0415 Å. The theoretical compressibility is 2.22 x 10^{-12} cm^2/dyne. Experimental values have been determined by Stephens and Lilley[10] of 2.88 x 10^{-12} cm^2/dyne, by Weil and Lawson[11] of 3.7 x 10^{-12} cm^2/dyne, and by Voronov et al[12] of 4.38 x 10^{-12} cm^2/dyne. The repulsive interactions were fitted to the exponential Born-Mayer form, $A \exp(-B r)$. The values of the repulsive parameters are listed in Table I.

Fischer et al determined the interactions between defect He^o and Li^o atoms and the host ions using a generalization of the semi-classical interaction

method developed by Wedepohl[13] using the charge densities for the Li^+ and H^- given above. The method is described in general in Appendix I, where the details of the He^o and Li^o interaction calculations are also given. The values of the parameters are listed in Table I. The interaction for the Li_2^+ molecule was taken from the work of Fischer and Kemmey.[14]

Table I Repulsive Interactions In LiH

Interaction	A in eV	B in A^{o-1}
$Li^{+}-H^{-}$	257.	3.24
$H^{-}-H^{-}$	29.3	1.88
$Li^{+}-Li^{+}$	1610.	7.29
$He^{o}-H^{-}$	151.	2.94
$He^{o}-Li^{+}$	616.	5.07
$Li^{o}-H^{-}$	11.2	1.52
$Li^{\delta}-Li^{+}$	63.4	1.94

Interactions are of the Born-Mayer form, A exp(-B r).

III. Method of Defect Calculations

The energy of a defect crystal relative to the energy of the perfect crystal, and the displacements of the ions surrounding the defect were calculated using an extension of the method of Hatcher and Dienes.[15] In the model employed, the crystal is made up of point, polarizable ions, and is divided into two regions. Region I contains the defect and a number of surrounding ions that are allowed to displace and polarize. Region II begins at the boundary of Region I and contains additional ions that are allowed to polarize, but not to relax. The energy of formation of a defect is written as the sum of electrostatic, repulsive, and polarization contributions:

$$E_{def} = E_{stat} + E_{rep} + E_{pol} \qquad (3)$$

each relative to the perfect crystal. The energy is minimized with respect to the displacements of the ions in Region I.

The electrostatic energy is given by:

$$E_{stat} = \sum_{i,j} \frac{e_i e_j}{r'_{ij}} - \frac{e_i e_j}{r_{ij}} \qquad (4)$$

where the sum is over all ions in the crystal, e_i and e_j are the charges of ions i and j, r'_{ij} is the distance between ions i and j in the defect crystal, and r_{ij}

is the distance between the ions in the perfect crystal. The prime on the summation indicates that the sum is not taken when i = j.

The repulsive interactions are made up of two body central forces of the Born-Mayer form, $A_{ij} \exp(-B_{ij} r_{ij})$ with the parameters listed in Section II. The repulsive energy is given by:

$$E_{rep} = \sum_{i,j}{}' A_{ij} \exp(-B_{ij} r'_{ij}) - A_{ij} \exp(-B_{ij} r_{ij}) \tag{5}$$

where the sum is over all ions in the crystal, but not when i = j.

The polarization energy is given by:

$$E_{pol} = -\tfrac{1}{2} \sum_{i} \bar{p}_i \cdot \bar{E}_i^{chg} \tag{6}$$

where the sum is over all polarizable ions, $\bar{p}_i$ is the induced electronic dipole on ion i due to the field of the charges and dipoles external to it, and $\bar{E}_i^{chg}$ is the monopole electric field at ion i due to the asymmetrical distribution of point charges around it. The total field at ion i is the field due to monopoles and dipoles external to ion i:

$$\bar{E}_i^{tot} = \bar{E}_i^{chg} + \bar{E}_i^{dip} \tag{7}$$

The induced electronic dipole on ion i is given by:

$$\bar{p}_i = \alpha_i \bar{E}_i^{tot}$$

$$= \alpha_i \bar{E}_i^{chg} + \alpha_i \bar{E}_i^{dip}$$

$$= \alpha_i \bar{E}_i^{chg} + \alpha_i \sum_j \frac{3\bar{r}_{ij}(\bar{p}_j \cdot \bar{r}'_{ij})}{r'^5_{ij}} - \frac{\bar{p}_j}{r'^3_{ij}} \qquad (8)$$

where α_i is the polarizability of ion i and the sum over j is over all dipoles but i. Eq. (8) holds for all dipoles and this set of simultaneous equations may be solved for the individual dipoles which can then be used in Eq. (6) to obtain the polarization energy.

Depending on the symmetry of the defect crystal the ions may be grouped into shells in which the ions have similar displacements and dipoles. This greatly simplifies finding the minimum energy configuration and also the computer time needed to solve the set of linear equations in (8).

This method avoids approximations used in other defect calculations.[16] Large regions of the crystal may be treated atomistically. The dipoles are solved for exactly in the region allowed to polarize and there is no need to use a polarizable continuum. Nonradial relaxations are allowed.

In practice from 50 to 60 ions were allowed to relax and polarize (Region I). For charged defects an additional 50 to 60 ions were allowed to polarize to account for long range polarization effects (Region II). Eight symmetry

types of defects were investigated: vacancy, divacancy, dinegative vacancy, quadrivacancy, body center interstitial, face center interstitial, (111) saddle point for interstitialcy migration, and (110) saddle point for interstitialcy migration. The ions used and their grouping into equivalent shells is given in Appendix II. The defects are illustrated in Figure 1.

The polarizability of the Li^+ (0.029 Å^3) was taken from Tessman, Kahn, and Schockley.[17] There is a large uncertainty in the value of the H^- polarizability - many widely varying values are reported in the literature.[7] The polarizability of the H^-, α_{H^-}, used in this work was determined from the Lorentz-Lorenz relation:

$$\frac{n^2 - 1}{n^2 + 2} = \frac{2\pi}{3} \left(\alpha_{Li^+} + \alpha_{H^-} \right) \qquad (9)$$

where r_o is the interionic distance and n is the refractive index (= 1.984) taken from Pretzel et al.[3] The resulting value is 1.93 Å^3 which is much smaller than the free ion polarizabilities reported in the literature. Pauling[18] has shown that the polarizability of two electron screened hydrogenic wave functions is proportional to the inverse fourth power of the screening parameter, $\alpha \sim \frac{1}{\zeta^4}$. The crystalline H^- ion used in II ($\zeta = .9$) therefore should have a smaller polarizability than the free ion ($\zeta = .6875$).

If the polarizability is held constant as the ions come closer together the defect calculations can yield unphysical results. The energy grows to unreasonably large

Figure 1

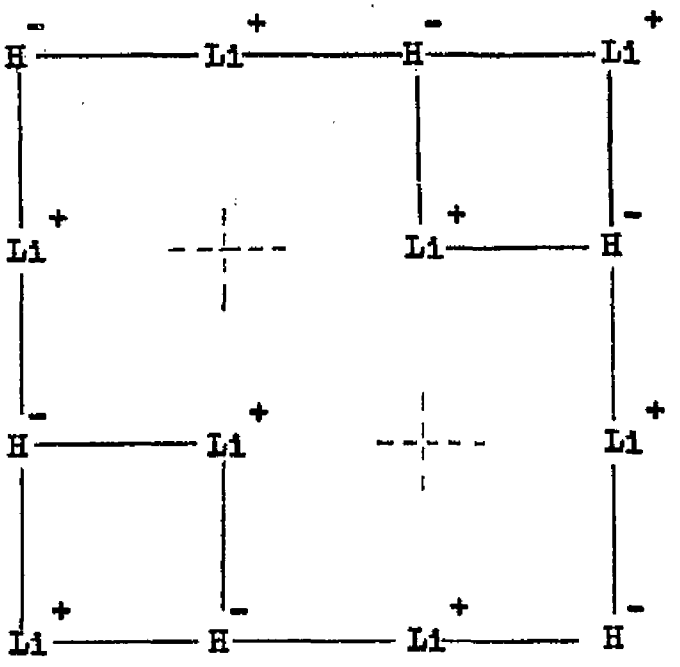

Dinegative Vacancy

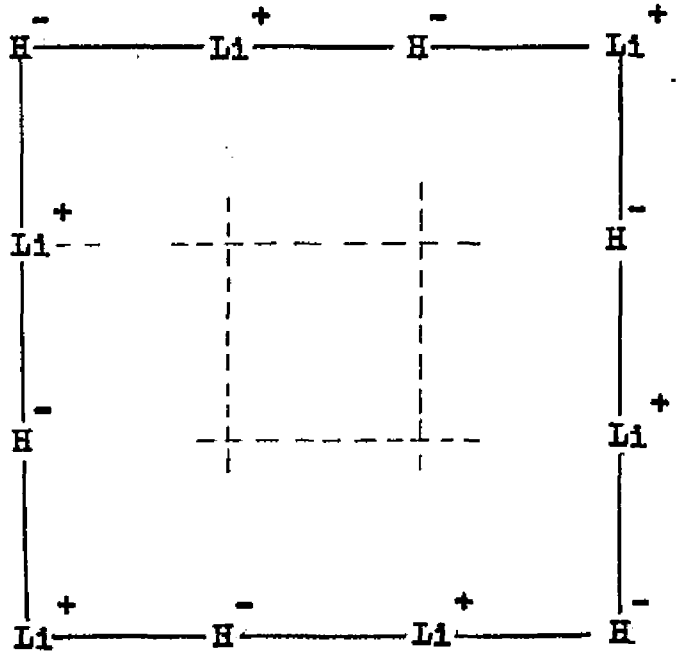

Quadrivacancy

Figure 1 (Continued)

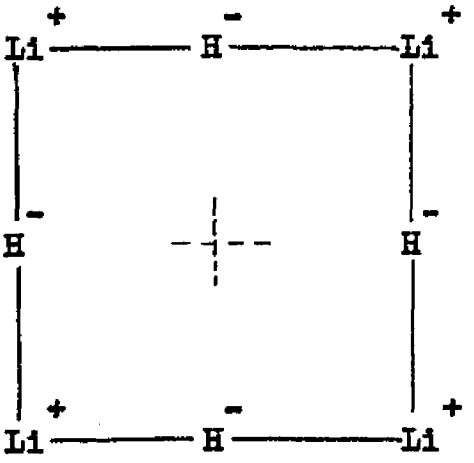

Positive Vacancy

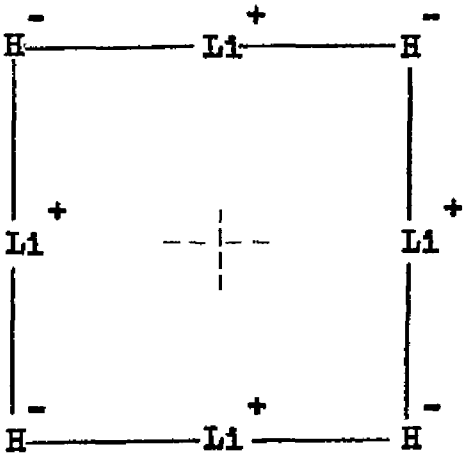

Negative Vacancy

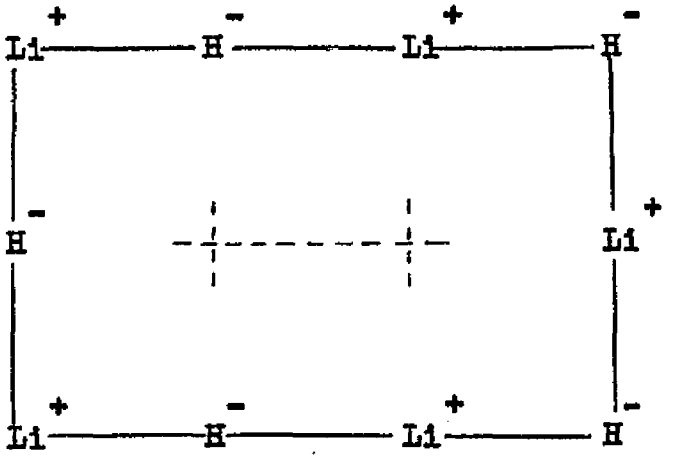

Divacancy

Figure 1 (continued)

Body Center Interstitial

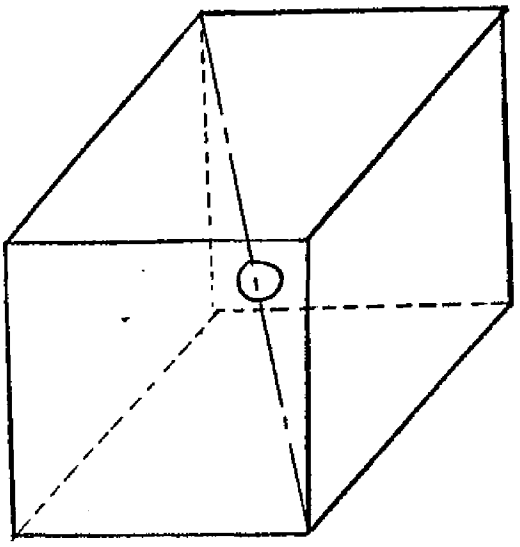

Face Center Interstitial

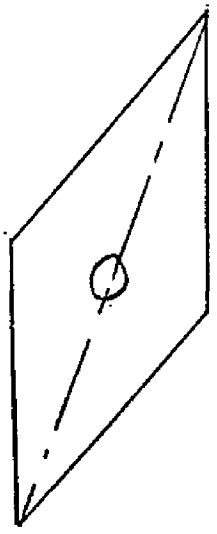

(111) Saddle Point for Interstitialcy Migration

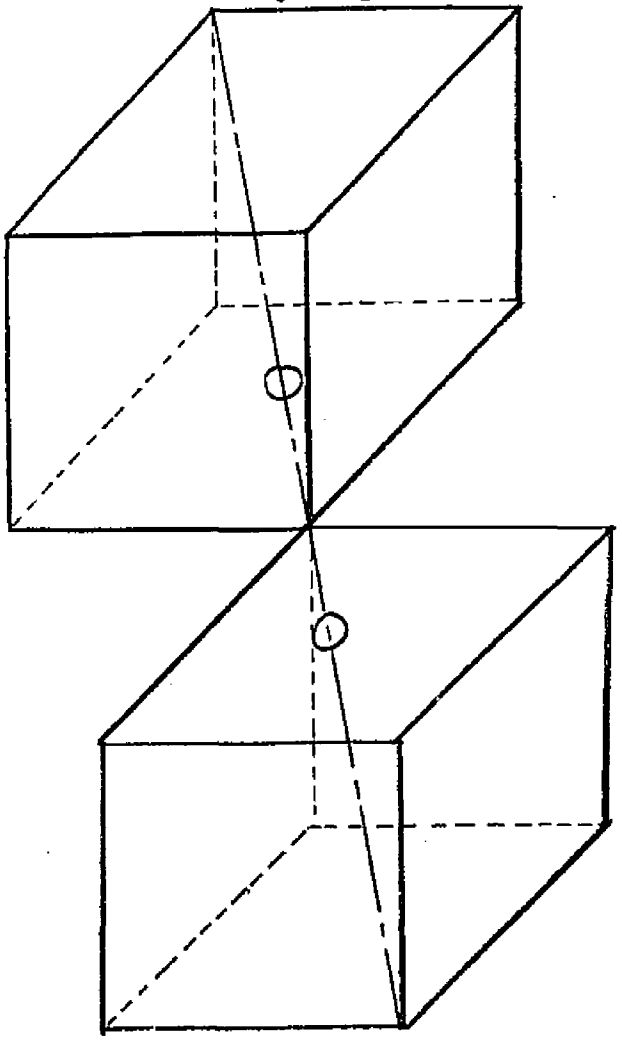

(110) Saddle Point for Interstitialcy Migration

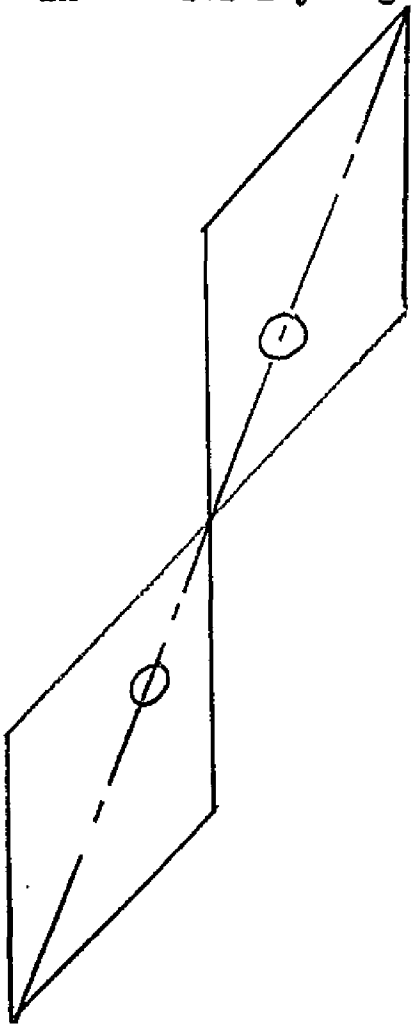

negative values. The interaction between a point charge, q, and a point dipole, polarizability α, at a separation r is $-\alpha q^2/r^4$ and this can overcome the Born-Mayer repulsion between the ions. This type of difficulty has been found in other ionic crystals. Scholz[19] has found this type of instability for defects in the lithium halides and Quigley and Das[20] have found this problem with off-center Li^+ in KCl. Yamashita and Kurosowa[21] had to arbitrarily reduce the value of the anion polarizability in the alkaline earth oxides in order to obtain agreement with the experimental value of the Schottky pair energy. In a recent review article Barr and Lidiard[22] have noted that in defect calculations with constant polarizabilities the results are usually below the experimental values indicating that the polarization is too great. They point out that it is reasonable that the polarizability decreases as the ions overlap. Indeed, this is what Quigley and Das did to correct the polarization energy.

The variation of the polarizability as a function of the separation between the ions has been considered by Goldberg,[23] who has done a quantum mechanical study of the effect of the crystalline environment on polarizabilities, and while the results are not directly applicable to this study he has shown that the polarizability decreases rapidly as the ions come together. Some simplified systems can be investigated. Consider a model of an ion in which a nuclear charge + Z e is surrounded by a

spherical charge distribution of radius a_o and total negative charge -Q e. Classically, the polarization of such an ion is given by:[24]

$$\alpha = a_o^3 \frac{Q}{Z} \tag{10}$$

Given two of these ions, A, B with radii a_o, b_o then when their internuclear separation, r, is such that $r > (a_o + B_o)$, the polarizabilities of the ions are given by Eq. (13). The point dipole model implies, as far as calculating the polarization is concerned, that the electron distributions do not overlap. Therefore, when $r < (a_o + b_o)$, it is assumed that the ions still contain uniform spherical charge distributions of total charge Q but that the radii contract to a and b, respectively, such that a + b = r and that a and b are in the same ratio as a_o and b_o. This means:

$$a = \frac{r}{a_o + b_o} a_o \tag{11}$$

When this radius is used in (10) the polarizability decreases as r^3 when $r < (a_o + b_o)$. A similar calculation was carried out but with exponentially decreasing charge densities instead of constant charge densities. This is the functional form of the charge distributions for the screened hydrogenic wave functions used in the model of repulsive interactions. The polarizabilities are still constant when $r > (a_o + b_o)$. When $r < (a_o + b_o)$ the

polarizability in this case depends on a convergent power series starting with terms in r^3, r^4, and r^5.

It is assumed that the polarizability of an H^- ion is a function of the positions of the ions surrounding it. When the nearest ion to an H^- is at the equilibrium separation r_o or greater the polarizability has the constant value given by the Lorentz-Lorenz relation, Eq. (9). When an ion comes closer to the H^- than r_o it is assumed that the polarizability decreases as r^4, such that at $r = 0, \alpha = 0$, and at $r = r_o$, $\alpha = 1.93$ A^3_o.

IV. Defects in Lithium Hydride:Lithium Tritide

In order to deduce the mechanism for low temperature volume expansion of LiH:LiT twenty-four defects were studied. The cases considered are: 1) Li^+ body center interstitial, 2) Li^+ face center interstitial, 3) Li^+ saddle point for (111) migration, 4) Li^+ saddle point for (110) migration, 5) H^- body center interstitial, 6) H^- face center interstitial, 7) H^- (111) saddle point, 8) H^- (110) saddle point, 9) positive vacancy, 10) negative vacancy, 11) divacancy, 12) dinegative vacancy, 13) quadrivacancy, 14) saddle point for positive vacancy migration, 15) saddle point for negative vacancy migration, 16) He^o body center interstitial, 17) He^o face center interstitial, 18) He^o on a negative vacancy, 19) He^o on a divacancy, 20) He^o on a dinegative vacancy, 21) He^o on a quadrivacancy, 22) Li^o body center interstitial, 23) Li^o face center interstitial, and 24) Li_2^+ on cation site oriented along (111). In Appendix III the details of the contributions to the total formation energy and the displacement parameters for relaxations about the defects are given. Table II summarizes the energies of the defects relative to the perfect crystal. Table III gives the activation energy for migration for the various diffusing ions and atoms to be described below.

Li^+ interstitials have the lowest energy in the body center position. By subtracting the energy in the

Table II

Energy of Defects Relative to the Perfect Crystal

1.	Li^+ Body Center Interstitial	-3.8 eV
2.	Li^+ Face Center Interstitial	-3.3
3.	Li^+ (111) Saddle Point	-3.5
4.	Li^+ (110) Saddle Point	-3.2
5.	H^- Body Center Interstitial	-2.4
6.	H^- Face Center Interstitial	-1.2
7.	H^- (111) Saddle Point	-2.9
8.	H^- (110) Saddle Point	-2.2
9.	Positive Vacancy	6.3
10.	Negative Vacancy	5.3
11.	Divacancy	9.0
12.	Dinegative Vacancy	13.2
13.	Quadvacancy	16.6
14.	Saddle Point for Li^+ Vacancy Migration	6.2
15.	Saddle Point for H^- Vacancy Migration	5.4
16.	He^0 Body Center Interstitial	.2
17.	He^0 Face Center Interstitial	.8
18.	He^0 on Negative Vacancy	5.6
19.	He^0 on a Divacancy	6.3
20.	He^0 on a Dinegative Vacancy	13.5
21.	He^0 in Quadvacancy	16.7
22.	Li^0 Body Center Interstitial	3.7
23.	Li^0 Face Center Interstitial	4.9
24.	Li_2^+ on a Cation Site Oriented Along (111)	1.4

Table III

Activation Energy for Migration in LiH

Species	Direction	Activation Energy, eV
Li^+ Interstitial	(100)	0.5
	(111)	0.3
	(110)	0.1
H^- Interstitial	(100)	0.7
	(111)	0.5
	(110)	1.0
He^0 Interstitial	(100)	0.6
Li^0 Interstitial	(100)	1.2
Li^+ Vacancy	(110)	0.1
H^- Vacancy	(110)	0.1

body center case from the face center case the activation energy through the face, i.e. along the (100), is obtained. Two additional possibilities for migration were considered. In the first case a body center interstitial might move along the (111) and push an on-site Li^+ into the center of the diagonally adjacent body while the original interstitial ion occupies the vacated lattice site. The saddle point for this interstitialcy migration is shown in Figure 2 and by comparing the energy in this configuration with the body center case the activation energy for diffusion in this direction is calculated. In the second case, it is possible for a face center interstitial to move along the (110) in a similar manner, and by investigating the saddle point the activation energy for migration along this direction is obtained. Li^+ has the lowest activation energy of all the interstitial ions and atoms investigated.

The energy of a crystal with a Li^+ interstitial is less than the energy of a perfect crystal and a free Li^+ at infinite separation. The increased electrostatic attraction and polarization due to the charged interstitial is greater than the additional repulsive interaction. To form an interstitial Li^+ in a perfect crystal a positive vacancy must also be formed. The formation energy of the Frenkel pair is 2.5 eV (sum of the energy of a positive vacancy, +6.8 eV, and the energy of the Li^+

body center interstitial, -3.8 eV). Therefore, LiH will not spontaneously form Li^+ interstitials.

The interstitial H^- ion has a lower energy in the (111) saddle point configuration than in the body center case. Tharmalingam[25] has found similar results for Cl^- interstitials in NaCl. The interstitial H^- also has a lower energy in the (110) saddle point than in the face center position. Therefore, in order to obtain the activation energy in the (100) direction the energy in the (111) saddle point case is subtracted from the energy in the (110) saddle point case. The energy of a negative vacancy is +5.3 eV and that of a H^- interstitial in the (111) saddle point is -2.9 eV. Therefore, the formation energy of anion Frenkel pairs is 2.4 eV.

The Schottky pair energy (sum of the formation energy of a positive vacancy, +6.3 eV, and a negative vacancy, +5.3 eV, minus the binding energy per ion pair, -9.69 eV) is 1.9 eV. The migration of either vacancy along the (110) has an activation energy of 0.1 eV. From conductivity data Pretzel et al[3] determined the experimental values of $2.4 \pm .2$ eV for the Schottky pair energy and $.53 \pm .5$ eV for the activation energy of the cation vacancy. The formation energy of a Schottky pair in LiH is less than the formation energy of either Frenkel pair indicating that the conductivity will be due primarily to vacancy migration in agreement with Pretzel's experimental results.

The clustering of vacancies into neutral pairs tends to reduce the electrical singularity of the isolated vacancies and is energetically favorable. The binding energy of a divacancy is 2.6 eV (the energy of the divacancy compared to the energy of separated positive and negative vacancies). The binding energy of the quadrivacancy considered is 1.4 eV (compared to two isolated divacancies). However, the charged dinegative vacancy is not bound and it is energetically favorable for it to dissociate into two isolated negative vacancies.

In the neighborhood of a vacancy ions of the same sign as the missing ion move away from the defect while ions of opposite sign move toward the defect.

He^{o} interstitials have a lower energy in the body center interstitial case than in the face center configuration. The theoretical activation energy for migration of He^{o} along the (100) is .6 eV. Based on the size and separation of He bubbles formed in damaged LiT crystals Jones[4] estimated the activation energy is of the order of .4 eV. The addition of a He^{o} to a negative vacancy, a dinegative vacancy, and a quadrivacancy raises the energy of these defects because of the increased repulsion between the host ions and the He^{o}. However, He^{o} is bound to a divacancy.

Li^{o} atoms have an activation energy of 1.2 eV. The Li^{o} may join with an on-site Li^{+} to form Li_2^{+} on an ion site which has a lower energy than the interstitial Li^{o}. The Li_2^{+} molecule is centered on a cation site

and oriented along the (111) direction.

V. Radiation Damage in Lithium Hydride:Lithium Tritide

The experimental work of Pretzel and Petty[4] demonstrated that the β particles were not responsible for the expansion. Pretzel[3] explained the low temperature expansion by assuming that the He^{o} formed in the β decay of the T^{-} goes into the body center interstitial position. The volume expansion can be determined from the relaxations about a body center He^{o} given in Table V. If p_1 amd p_2 are the components of the outward displacements for the interstitial's first nearest neighbors, measured in units of r_o, then the volume expansion of the cube containing the interstitial is given by:

$$V = r_o^3 (1 + p_1 + p_2)^3 - r_o^3 \qquad (12)$$

$r_o = 2.216\ \text{Å}^3$

The expansion for the interstitial He^{o} using (12) is 7 Å^3. From the experimental volume expansion data and the half life of the T^{-} Pretzel and Petty determined that an expansion of 12.4 Å^3 per beta decay was needed to agree with experiment. Therefore, this mechanism is insufficient to explain the volume expansion.

Following Eshelby[27] the volume expansion may be calculated from continuum elastic theory. In a continuous isotropic elastic medium the relaxations around a spherically symmetric defect are given by:

$$\bar{d} = c \frac{\bar{r}}{r^3} \qquad (13)$$

where $\bar{d}$ is the radial displacement at a point a distance $\bar{r}$ from the defect and C is a constant measuring the "elastic strength" of the defect. The volume expansion in an infinite medium caused by this displacement field is:

$$V = 4\pi C \tag{14}$$

For a non-infinite medium surface effects must be taken into account and the volume expansion for a finite spherical medium containing the defect is:

$$V = 4\pi C \frac{3K + 4c_{44}}{3K} \tag{15}$$

where K is the compressibility and c_{44} is one of the elastic constants. The compressibility from II is 2.22×10^{-12} cm^2/dyne and c_{44} is $.48 \times 10^{27}$ $^{-12}$ cm^2/dyne.

In Table V are listed the relaxations for 136 ions around a body center interstitial He^o. For each shell the radial displacement was calculated and a value of C was determined using Eq. (13). The C's for all the shells were averaged taking the multiplicity of the shells into account and the value C=.047 obtained. The resulting volume expansion using eq. (15) is 8 A^{o3}, in good agreement with the value calculated by Eq. (12) and still insufficient to explain the volume expansion.

When the T^- decays and emits the β the He^o recoils. The average recoil energy is 1.04 eV and the maximum recoil energy is 3.28 eV. It is possible that in recoiling the He^o might collide with one of the surrounding Li^+

Table V Displacements Around a Body Center Interstitial He°

Shell	Multiplicity	Typical Ion Position x	y	z	Displacement x	y	z
1	1	0	0	0	0	0	0
2	4	0.5	0.5	0.5	.11	.11	.11
3	4	0.5	-0.5	0.5	.08	-.08	.08
4	12	1.5	0.5	0.5	-.01	.03	.03
5	12	1.5	0.5	-0.5	-.04	.10	-.10
6	12	1.5	1.5	-0.5	.01	.01	-.025
7	12	1.5	0.5	0.5	-.06	-.06	.06
8	4	1.5	1.5	1.5	-.005	-.005	-.005
9	4	1.5	1.5	-1.5	-.01	-.01	.01
10	12	2.5	0.5	-0.5	.005	.01	-.01
11	12	2.5	0.5	0.5	.01	.02	.02
12	24	2.5	1.5	0.5	.01	-.01	.005
13	24	2.5	1.5	-0.5	.04	-.02	.015

Shell 1 is the interstitial. The Displacement gives the components of the displacement vector of the Typical Ion about its normal lattice site. The ion at (.5,.5,.5) is a Li^+.

or H^- ions and transfer some of its energy. In Table IV the maximum energy transferable in an elastic collision between the recoiling He^o atom and the host ions is presented.

A possible mechanism for the low temperature volume expansion is suggested in Figure 2. In (a) a T^- ion is about to undergo β decay. In (b) the decay has just occured and the recoiling He^o atom collides with one of its six nearest neighbor Li^+ ions and transfers some of its energy. From Table IV it is seen that for a He^o atom with average recoil energy the Li^+ could receive up to . 85 eV of energy. Because of the low activation energy for the Li^+ (.1 eV along the (110)) it is probable that in many of the collisions the Li^+ will displace several lattice constants away from its site and become a body center interstitial as is shown in (c). The immediate result of the beta decay is to have a He^o on a negative ion site with no relaxation of the surrounding ions which raises the energy of the crystal 7.8 eV. The energy difference comes from the nuclear energy of the β decay. The energy of the resultant He^o in a divacancy (6.3 eV) and the body center interstitial Li^+ (-3.8 eV) is 2.5 eV and therefore the reaction is energetically favorable. The relaxations of the ions surrounding the Li^+ interstitial are given in Table VII. The volume expansion using Eq. (12) is 5 A^{o3} and from Eq. (15) is 12 A^{o3}. This is still not quite sufficient to explain the observed volume expansion.

The Li^+ will attract and capture one of the electrons

Table IV

Maximum Energy Transferable in an Elastic Collision with an He^0

Ion	Mass	He^0 energy	
		1.04 eV	3.28 eV
H^-	1	0.78eV	2.46 eV
T^-	3	1.04	3.28
Li^+	6	0.93	2.92
Li^+	7	0.85	2.76

When a T^- decays into He^o, the He^o acquires an average of1.04 eV and a maximum of 3.28 eV of recoil energy. When the He^o with mass m_{He} and energy E_{He} collides with an ion of mass m_i at rest the maximum energy transferrable to the ion E_i is given by:

$$E_i = \frac{4\, m_{He}\, m_i}{(m_{He} + m_i)^2} E_{He}$$

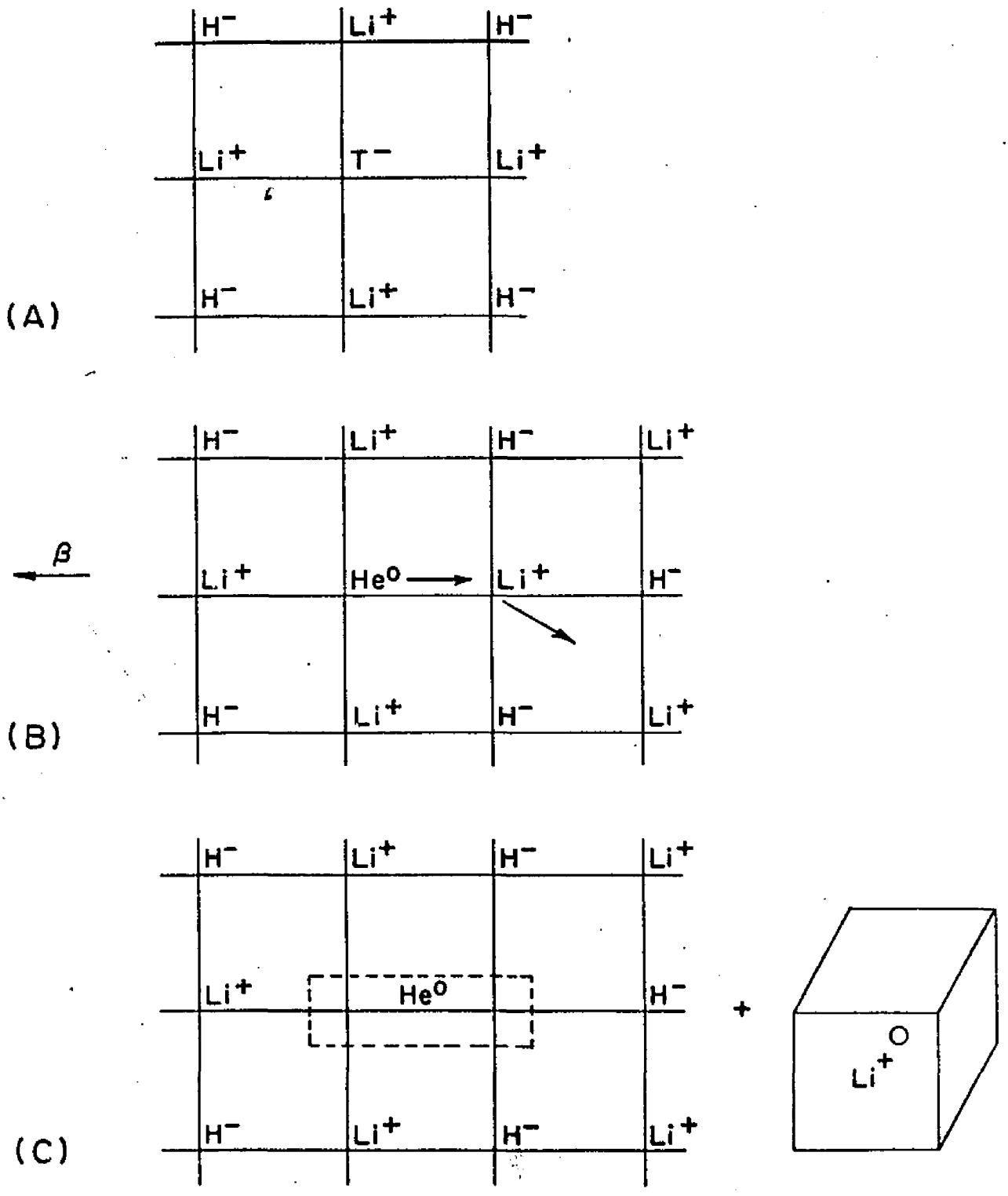
H⁻
Li⁺
H⁻
Li⁺
T⁻
Li⁺
H⁻
Li⁺
H⁻
(A)
β
H⁻
Li⁺
H⁻
Li⁺
Li⁺
He⁰
Li⁺
H⁻
H⁻
Li⁺
H⁻
Li⁺
(B)
H⁻
Li⁺
H⁻
Li⁺
Li⁺
He⁰
H⁻
H⁻
Li⁺
H⁻
Li⁺
(C)
+
O
Li⁺

Figure 2

Table VII Displacements Around a Body Center Interstitial Li+

Shell	Multiplicity	Typical Ion Position x	y	z	Displacements x	y	z
1	1	0	0	0	0	0	0
2	4	0.5	0.5	0.5	.15	.15	.15
3	4	0.5	-0.5	0.5	-.01	-.01	-.01
4	12	1.5	0.5	0.5	0	.03	.03
5	12	1.5	0.5	-0.5	-.01	.05	-.05
6	12	1.5	1.5	-0.5	-.02	-.02	-.01
7	12	1.5	1.5	0.5	.01	.01	.04
8	4	1.5	1.5	1.5	.01	.01	.01
9	4	1.5	1.5	-1.5	0	0	0
10	12	2.5	0.5	-0.5	0	.01	-.01
11	12	2.5	0.5	0.5	.03	.055	.055
12	24	2.5	1.5	0.5	.005	-.005	.01
13	24	2.5	1.5	-0.5	.035	-.035	-.035

from the β decay. The ionization energy of the Li^{o} atom in the LiH crystal can be obtained by considering a cycle similar to the one used by Dienes and Smolouchowski[28] to estimate the electron affinity of Cl^{o} in NaCl:

(a) Li^{o}(crystal) $\rightarrow$ Li^{o}(free) $\quad \Delta U = -3.7$ eV

(b) Li^{o} (free) $\rightarrow$ Li^{+}(free) + e^{-}(free) $\quad \Delta U = 5.36$

(c) Li^{+}(free) $\rightarrow$ Li^{+}(crystal) $\quad \Delta U = -3.8$

(d) e^{-}(free) $\rightarrow$ e^{-}(crystal) $\quad \Delta U = 0$

(e) Li^{+}(crystal) + e^{-}(crystal) $\rightarrow$ Li^{o}(crystal) $\quad \Delta U = X$

$\Sigma \Delta U = 0$

In (a) a Li^{o} body center interstitial is removed from the crystal with an energy change of -3.7 eV. In (b) the free Li^{o} is ionized and the change in energy is the normal ionization energy. In (c) the Li^{+} is put back in the body center interstitial position with a gain in energy of 3.8 eV. In (d) the electron is brought back from infinity to the bottom of the conduction band. This energy change will be small and taken as zero. In (e) the Li^{+} in the crystal and the electron in the conduction band join and the change in energy, X, is the negative of the ionization energy in the crystal. The cycle is now complete and the net change in energy is zero. The ionization energy calculated from this cycle is -2.2 eV indicating that the Li^{o} is unstable against dissociation into an interstitial Li^{+} ion and an e^{-} in the conduction band. The Li^{o} may still be

metastable however. In Table VI are presented the relaxations for 136 ions surrounding a body center Li^{o}. The expansion using Eq. (12) is 14 $\mathring{A}^3$ and using (15) is 19 $\mathring{A}^3$.

The Li^{o} could stabalize by forming a Li_2^+ molecule ion on an anion lattice site. The Li_2^+ (1.4 eV) is 2.3 eV lower in energy than the Li^{o} and considering the same type of cycle would be stable by .1 eV. The volume expansion of a sphere drawn through the first nearest neighbors of the Li_2^+ is 12 $\mathring{A}^3$ using the relaxations given in Table VIII. The Li_2^+ is not a spherically symmetric defect and the calculation of the volume expansion by continuum elastic theorey is more complicated. Townsend[26] has solved the problem of the relaxations around a linear defect in an isotropic medium. The displacement field is given by:

$$\bar{d} = \frac{C\,\bar{r}}{r^3} + \frac{D\,\bar{r}}{r^3}(3\cos^2\Theta - 1) - \frac{C}{r^2}\,3\sin\Theta\cos\Theta\,\hat{\lambda}_\Theta \qquad (14)$$

where $\bar{d}$ is the displacement at a distance $\bar{r}$ from the center of the defect and making an angle Θ with the axis of the defect, $\hat{\lambda}_\Theta$ is a unit vector in the Θ direction, and $D = 30(3 + 3Kc_{44})/6c_{44}K$. Only the first term on the left of Eq. (16), the purely radial term, contributes to the volume expansion and the total expansion including surface effects is given by Eq. (15). The displacements about the Li_2^+ were resolved into radial and angular components and the value of C was determined for each shell. The average value of C = .0838. The expansion from Eq. (15) is 14 $\mathring{A}^3$ which is sufficient to explain the volume expansion. observed.

Table VI Displacements Around a Body Center Interstitial Li°

Shell	Multi-plicity	Typical Ion Position x	y	z	Displacements x	y	z
1	1	0	0	0	0	0	0
2	4	0.5	0.5	0.5	.21	.21	.21
3	4	0.5	-0.5	0.5	.10	-.10	.10
4	12	1.5	0.5	0.5	.02	.05	.05
5	12	1.5	0.5	-0.5	-.04	.09	-.09
6	12	1.5	1.5	-0.5	.03	.03	-.02
7	12	1.5	1.5	0.5	.02	.02	.04
8	4	1.5	1.5	1.5	.02	.02	.02
9	4	1.5	1.5	-1.5	.02	.02	-.02
10	12	2.5	0.5	-0.5	.005	0	0
11	12	2.5	0.5	0.5	.02	-.005	-.005
12	24	2.5	1.5	.5	.005	.005	0
13	24	2.5	1.5	-0.5	.015	.005	-.015

Table VIII Displacements Around a Li_2^+

Shell	Multiplicity	Typical Ion Position x	y	z	Displacements x	y	z
1	2	0	0	0	0	0	0
2	6	1	0	0	.08	0	0
3	6	1	1	0	.14	.14	-.06
4	6	1	0	-1	-.06	0	.06
5	2	1	1	1	0	0	0
6	2	1	1	-1	.04	.04	.03
7	6	2	0	0	-.01	-.011	-.011
8	12	2	1	0	0	.04	-.005
9	12	2	0	-1	.03	-.035	-.01
10	6	2	1	1	-.035	.045	.045
11	12	2	1	-1	-.02	.06	.005
12	6	2	-1	-1	.07	-.035	-.035
13	6	2	2	0	-.02	-.02	-.01
14	6	2	-2	0	.025	-.025	0
15	6	3	0	0	0005	.005	.005
16	6	2	2	1	-.005	-.005	.02
17	6	2	2	-1	.01	.01	-.015

The formation of the Li_2^+ would explain the paramagnetic resonance observed in expanded crystals. The Li_2^+ can also serve as the nucleus for precipitation of Li metal in heavily damaged samples.

It is difficult to estimate the fraction of β decays that will result in interstitial lithium. Pretzel[3] assumed that the H^- in LiH has a radius of 1.4 Å and the He^o a radius of 1.0 Å. In the model used in this paper the Li^+ would then have a radius of 0.8 Å. Using a hard sphere model of the ions it would be impossible for the He^o to move off the site from which it was created without colliding with one of its six nearest neighbor Li^+ ions. The very low activation energy for Li^+ migration makes the displacement fairly easy.

The possibility of other mechanisms being present cannot be excluded. More than one Li^+ may be displaced by a recoiling He^o atom; a Li^+ may be displaced even though the He^o goes into an interstitial position; or the ions displaced by the He^o may not be those adjacent to the site where it was created.

In Figure 3 a similar mechanism involving the H^- is considered. The T^- in (a) undergoes β decay and in (b) it collides with one of its twelve next nearest neighbor H^- ions and transfers some of its energy. It is less probable for the H^- to displace in a collision with the He^o than the Li^+ because of its higher activation energy. In (c) is shown the resulting He^o in a dinegative vacancy (13.5 eV) and the interstitial H^- (-2.9 eV). The final energy is 10.6 eV

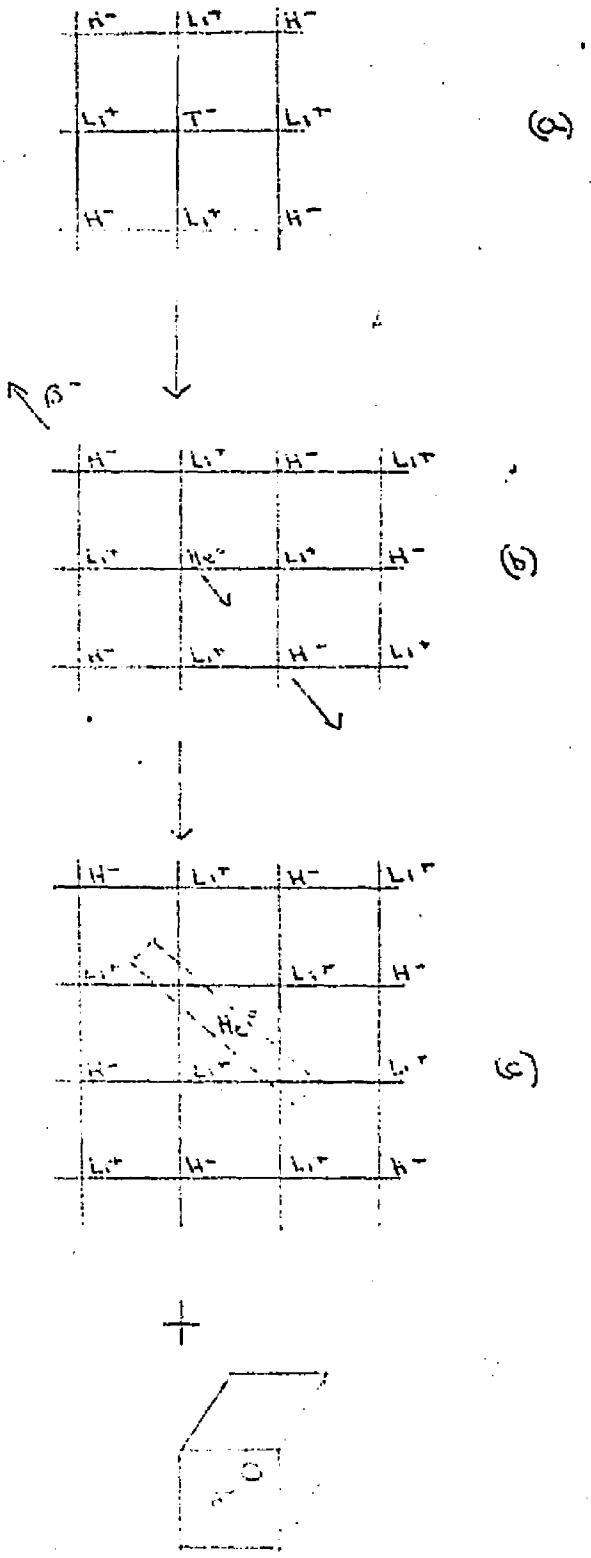

Figure 3

which is considerably higher than the 7.8 eV of the He^{o} on the negative ion site which started this mechanism. Pretzel and Petty[4] have presented arguements to show that if interstitial H^{-} is formed it would join with an on-site anion to form H_2. Since no hydrogen gas is observed at low temperatures this adds support to the theoretical prediction that no interstitial H^{-} ions are formed. Therefore, the displacement sequence is energetically unfavorable for the H^{-} at low temperatures.

As noted in I, the high temperature radiation damage in LiH:LiT is much more complicated. Some comments on this temperature range can be made. The binding energies of the divacancy and quadrivacancy indicate the clustering of vacancies is energetically favorable and would help explain the voids observed at high temperatures. A possible mechanism for the formation of H_2 at high temperatures is shown in Fig. 4. Again, in (a) a T^{-} ion is about to undergo β decay and in (b) the recoiling He^{o} collides with one of its twelve next nearest neighbor H^{-} ions. Because of the high temperature it is very easy for the H^{-} to displace and the products shown in (c) result. The two nearest Li^{+} ions to the He^{o} in the dinegative vacancy are displaced considerably off-site away from the defect. At these elevated temperatures it is possible for these two Li^{+} ions to migrate away leaving a He^{o} in a quadrivacancy (16.7 eV), the two Li^{+} interstitials (-3.8 eV each), and the H^{-} interstitial (-2.9 eV) is less than the energy of the He^{o} on the negative vacancy (7.8 eV). The H^{-} would now form H_2 by the arguements of Pretzel and Petty.

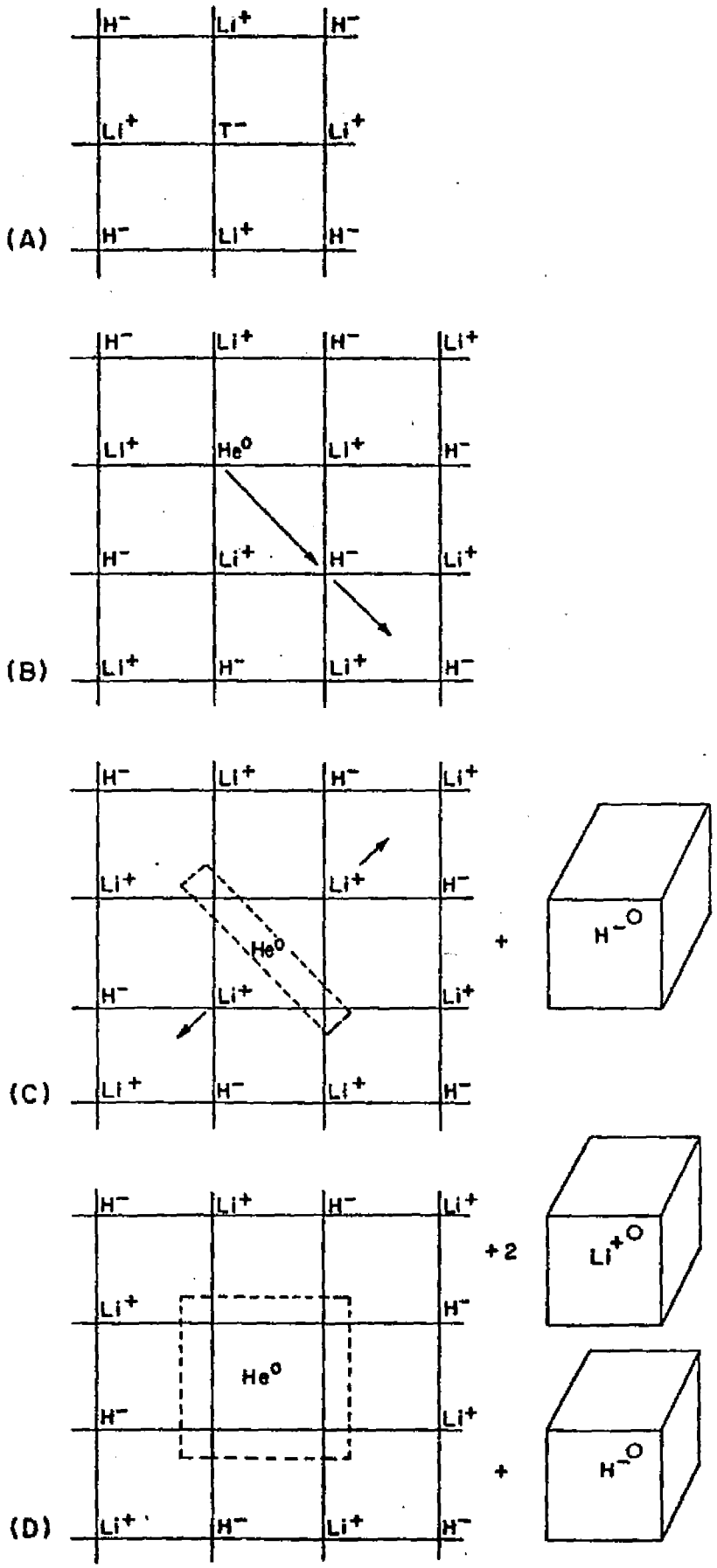
(A)
H⁻ Li⁺ H⁻
Li⁺ T⁻ Li⁺
H⁻ Li⁺ H⁻
(B)
H⁻ Li⁺ H⁻ Li⁺
Li⁺ He⁰ Li⁺ H⁻
H⁻ Li⁺ H⁻ Li⁺
Li⁺ H⁻ Li⁺ H⁻
(C)
H⁻ Li⁺ H⁻ Li⁺
Li⁺ Li⁺ H⁻
He⁰
H⁻ Li⁺ Li⁺
Li⁺ H⁻ Li⁺ H⁻
+
H⁻O
(D)
H⁻ Li⁺ H⁻ Li⁺
Li⁺ H⁻
He⁰
H⁻ Li⁺
Li⁺ H⁻ Li⁺ H⁻
+2
Li⁺O
+
H⁻O

Figure 4

VI. Summary

The low temperature volume expansion of LiH:LiD has been theoretically investigated using a method for defect calculations utilizing a point polarizable ion model of LiH. Twenty-four defect calculations on LiH were performed and the results interpreted. The theoretical model of the low temperature volume expansion of Pretzel, involving an interstitial He^{o} atom, was shown to be inadequate in explaining the observed expansion. An alternate mechanism involving the formation of an interstitial Li_2^{+} molecule was suggested and shown to provide an explanation for the low temperature volume expansion. In addition, the mechanism accounts for the nucleation of metallic lithium and the presence of ESR signals. A mechanism for the formation of H_2 was proposed and found to be unfavorable at low temperature, but possible at high temperatures in agreement with the experimental results.

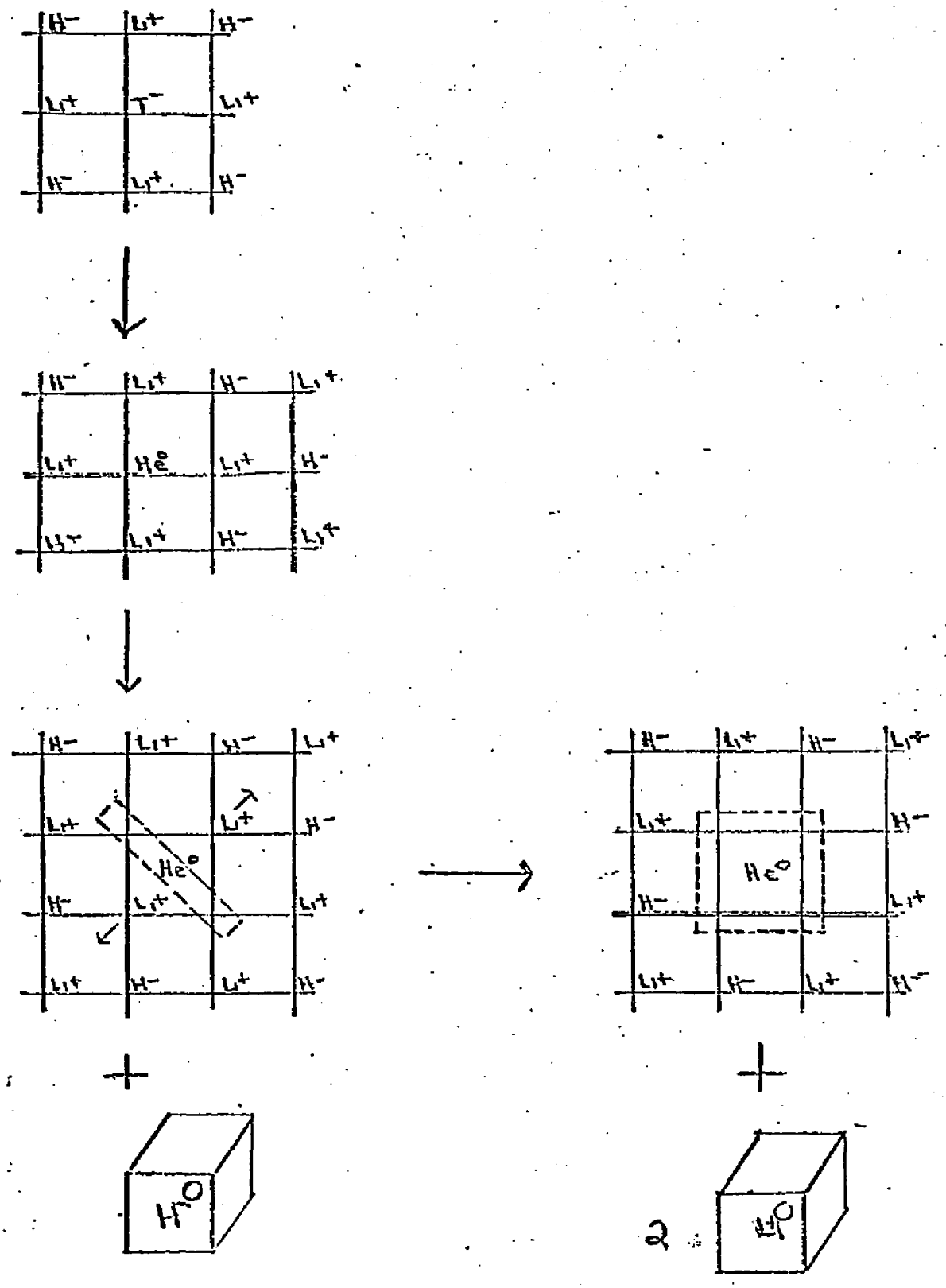

FIGURE 5 - HIGH TEMPERATURE H^- MECHANISM

Appendix I

1. Introduction

The diatomic quantum mechanical treatment of the repulsive interactions in LiH requires a considerable amount of computer time. For heavier ions the method may be impractical. A quicker approximate method might be useful provided it did not sacrifice too much in accuracy.

Approximate methods for calculating the interaction energy have been used by Firsov[1], Abrahmason et. al.[2], Abrahamson[3,4], and Wedepohl[5,6]. Firsov used the Thomas-Fermi approximation, Abrahamson used the Thomas-Fermi-Dirac method, and Wedepohl considered a general electron distribution. All three consider the interactions of similar atoms and, in addition, Wedepohl considers the interactions between like ions. In each case the kinetic energy is calculated as:

$$E_k = \frac{3}{5}\,\frac{\hbar^2\pi^2}{2m}\left(\frac{3}{\pi}\right)^{\frac{2}{3}}\int \rho^{5/3}\,d\tau \qquad (1)$$

where ρ is the electron density and the integral is over the charge distribution. Further, Abrahamson and Firsov use the Dirac formalism for the exchange energy:

$$E_a = \frac{3}{16\pi\epsilon_0}\left(\frac{3}{\pi}\right)^{\frac{1}{3}} e^2 \int \rho^{4/3}\,d\tau \qquad (2)$$

Both equations are derived for a degenerate electron gas and then applied to the atomic case. Therefore, this statistical approach should have a greater validity for heavier atoms.

As a first step towards obtaining an approximate method for the interactions we will generalize Wedepohl's work to include interactions between unlike ions and atoms.

2. Model

Atom or ion A (B) has a nuclear charge of $+Z_a$ e ($+Z_b$ e) surrounded by a spherically symmetric electron charge distribution $p_a(r_a)$ ($p_b(r_b)$) which contains Q_a (Q_b) electrons. The electron distribution has a finite radius a (b). As a convention it is assumed

$$b \geq a \qquad (3)$$

When the atoms interact it is assumed that the electron distributions do not distort and that each nucleus remains at the center of its electron distribution.

2. Terms in the Total Interaction Energy

The total interaction energy is written as:

$$E = E_{n_a n_b} + E_{e_a e_b} + E_{n_a e_b} + E_{n_b e_a} + E_k + E_a \qquad (4)$$

$E_{n_a n_b}$ is the electrostatic interaction between the two nuclei; $E_{e_a e_b}$ is the electrostatic interaction between the two electron distributions; $E_{n_a e_b}$ is the interaction

between the nucleus of A and electrons of B; $E_{\eta_b e_a}$ is the interaction between the nucleus of B and electrons of A; E_k is the increase in kinetic energy due to overlap; and E_a is the increase in exchange energy due to overlap. Rationalized mks units are used. Thus

$$E_{\eta_a \eta_b} = \frac{Z_a Z_b e^2}{4\pi\epsilon_0 r} \tag{5}$$

4. Calculation of the Electron-Electron Energy

Consider two elementary spherical shells, carrying uniformly distributed charges dq, dq' and having radii x and y. The force between the two shells for different distances between the centers, r, is given by:

$$r > |a+b| \qquad dF = \frac{dq\, dq'}{4\pi\epsilon_0 r^2} \tag{6}$$

$$|a+b| < r < |a-b| \qquad dF = \frac{dq\, dq'}{16\pi\epsilon_0 r^2}\left(2 + \frac{r^2}{xy} - \frac{x}{y} - \frac{y}{x}\right) \tag{7}$$

$$r < |a-b| \qquad dF = 0 \tag{8}$$

By using these formulas the force between the two spherically symmetric charge distributions can be calculated by integrating between the appropriate limits. There are five cases to consider.

(i) No overlap r a + b

$$F_{ee} = \frac{Q_A Q_B}{4\pi\epsilon_0 r^2} \tag{9}$$

The distributions behave like point charges.

(ii) $b < r < a + b$

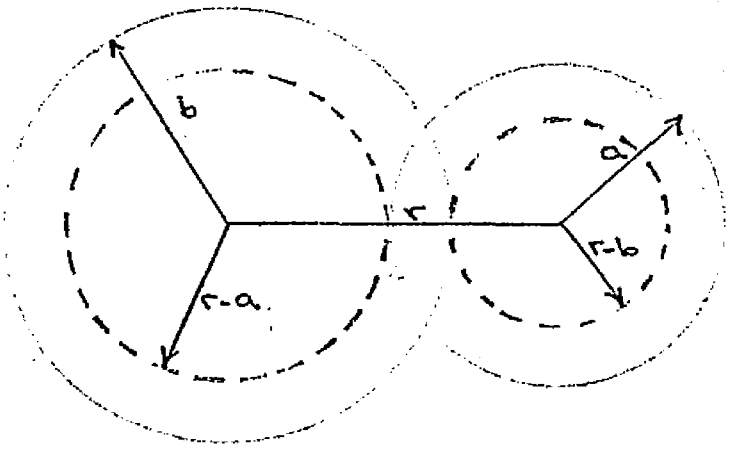

FIGURE 1.

In this case the repulsive force is given by

$$F_{ee} = \frac{e^2}{4\pi\epsilon_0 r^2}\left[Q_{SA}Q_B + Q_{SB}Q_A - Q_{SA}Q_{SB} + \int_{r-a}^{b} g(y)\,dy\left\{\int_{r-b}^{r-y} f(x)\,dx + \int_{r-y}^{a} \Phi(x,y) f(x)\,dx\right\}\right] \tag{10}$$

where

$$f(x) \equiv 4\pi x^2 \rho_a(x) \;;\quad g(y) \equiv 4\pi y^2 \rho_b(y) \tag{11}$$

and

$$\Phi(x,y) \equiv \frac{1}{4}\left(2 + \frac{r^2}{xy} - \frac{y}{x} - \frac{x}{y}\right) \tag{12}$$

Also Q_{sa} is the total electron charge of atom A in a sphere of radius r-b about nucleus A and Q_{sb} is the total electron charge of atom B in a sphere of radius r-a about nucleusB, i.e.:

$$Q_{SA} \equiv \int_0^{r-b} f(x)\,dx \tag{13}$$

$$Q_{SB} \equiv \int_0^{r-a} g(y)\,dy \tag{14}$$

(iii) $a < r < b$

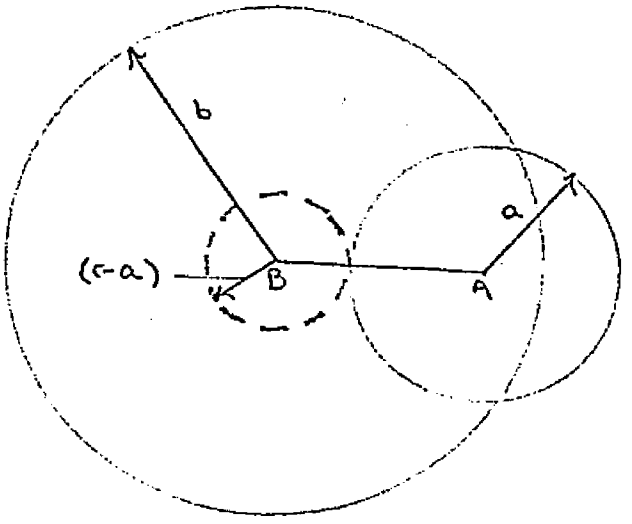

FIGURE 2

This case does not occur for identical ions. The force is:

$$F_{ee} = \frac{e^2}{4\pi\epsilon_0 r^2}\left[Q_{SB}Q_A + \int_{r-a}^{r} g(y)\,dy\left\{\int_0^{r-y} f(x)\,dx + \int_{r-y}^{a} f(x)\,\phi(x,y)\,dx\right\} + \int_r^b g(y)\,dy \int_{y-r}^{a} f(x)\,\phi(x,y)\right] \quad (15)$$

If the smaller sphere is inside the larger one $r < |a-b|$ then the limits of the last integral change:

$$F_{ee} = \frac{e^2}{4\pi\epsilon_0 r^2}\left[Q_{SB}Q_A + \int_{r-a}^{r} g(y)\,dy\left\{\int_0^{r-y} f(x)\,dx + \int_{r-y}^{a} f(x)\,\phi(x,y)\,dx\right\} + \int_r^{r+a} g(y)\,dy \int_{y-r}^{a} f(x)\,\phi(x,y)\,dx\right] \quad (16)$$

(iv) $a/2 \leq r \leq a$

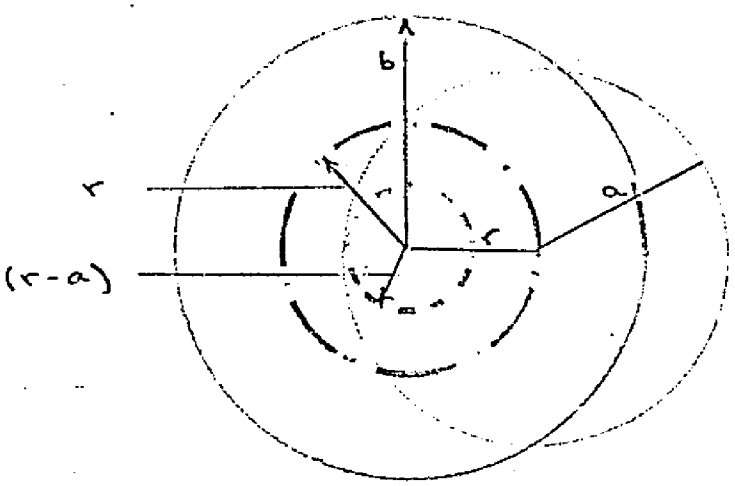

FIGURE 3

The force between the two electron distributions is

$$F_{ee} = \frac{e^2}{4\pi\epsilon_0 r^2}\Big[\int_0^r g(y)dy \int_0^{r-y} f(x)\,dx + \int_0^{r-a} g(y)dy \int_{r-y}^{r+y} f(x)\,\phi(x,y)\,dx + \int_{r-a}^{r} g(y)dy \int_{r-y}^{a} f(x)\,\phi(x,y)dx + \int_r^b g(y)\,dy \int_{y-r}^{a} f(x)\,\phi(x,y)dx \Big] \tag{17}$$

The dashed lines - - - in Figure 3 shows the limits of the second integration in (17) and the semi-dashed circle is the limits of the third integration. In addition, if one sphere is inside the other, $r < |b - a|$ the limits of the last integral change:

$$F_{ee} = \frac{e^2}{4\pi\epsilon_0 r^2}\Big[\int_0^r g(y)\,dy \int_0^{r-y} f(x)dx + \int_0^{r-a} g(y)\,dy \int_{r-y}^{r+y} f(x)\,\phi(x,y)\,dx + \int_{r-a}^{r} g(y)dy \int_{r-y}^{a} f(x)\,\phi(x,y)dx + \int_r^{r+a} g(y)\,dy \int_{y-r}^{a} f(x)\,\phi(x,y)dx \Big] \tag{18}$$

(v) $r \leq a/2$

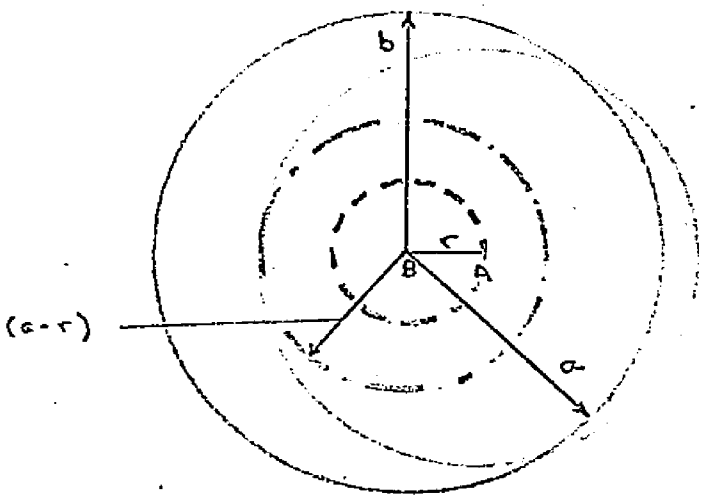

FIGURE 4

The force is:

$$F_{ee} = \frac{e^2}{4\pi\epsilon_0 r^2}\left[\int_0^r g(y)\,dy \int_0^{r-y} f(x)\,dx + \int_0^r g(y)\,dy \int_{r-y}^{r+y} f(x)\,\phi(x,y)\,dx + \int_r^{a-r} g(y)\,dy \int_{y-r}^{r+y} f(x)\,\phi(x,y)\,dx + \int_{a-r}^{b} g(y)\,dy \int_{y-r}^{a} f(x)\,\phi(x,y)\,dx\right] \quad (19)$$

Again if the smaller sphere is inside the larger, $r \leq |b - a|$ the limits on the last integral changes.

$$F_{ee} = \frac{e^2}{4\pi\epsilon_0 r^2}\left[\int_0^r g(y)\,dy \int_0^{r-y} f(x)\,dx + \int_0^r g(y)\,dy \int_{r-y}^{r+y} f(x)\,\phi(x,y)\,dx + \int_r^{a-r} g(y)\,dy \int_{y-r}^{r+y} f(x)\,\phi(x,y)\,dx + \int_{a-r}^{r+a} g(y)\,dy \int_{y-r}^{a} f(x)\,\phi(x,y)\,dx\right] \quad (20)$$

The electron-electron interaction energy is calculated by integrating the force from the internuclear separation, r, to a + b:

$$E_{ee} = \frac{Q_a Q_b e^2}{4\pi\epsilon_0 (a+b)} + \int_r^{a+b} F_{ee}(r')\, dr' \qquad (21)$$

The first term is just the value of E_{ee} when r = a + b.

5. Calculation of the Electron Nuclear Interactions

When $r > b$ nucleus A is outside electron distribution B and the interaction energy is

$$E_{n_a e_b} = \frac{-Q_b Z_a e^2}{4\pi\epsilon_0 r} \qquad (22)$$

When $r < b$ the force between nucleus A and electrons B is that between nucleus A and a point charge at B whose charge equals the electronic charge in a sphere of radius r about B:

$$F_{n_a e_b} = \frac{-Z_a e^2}{4\pi\epsilon_0 r^2} \int_0^r 4\pi y^2 \rho_b(y)\, dy \qquad (23)$$

The energy is given by:

$$E_{n_a e_b} = -\frac{Z_a e^2}{4\pi\epsilon_0}\left[\frac{Q_b}{b} + \int_r^b \frac{1}{r'^2}\left\{\int_0^{r'} 4\pi y^2 \rho_b(y)\, dy\right\} dr'\right] \qquad (24)$$

Similarly:

$$E_{n_b e_a} = -\frac{Z_b e^2}{4\pi\epsilon_0}\left[\frac{Q_a}{a} + \int_r^a \frac{1}{r'^2}\left\{\int_0^{r'} 4\pi y^2 \rho_a(y)\, dy\right\} dr'\right] \qquad (25)$$

6. Calculation of the Kintetic and Exchange Energies

From (1) the increase in the kinetic energy due to overlap is given by:

$$E_k = K_k \int \left\{ (\rho_a(r) + \rho_b(r))^{5/3} - \rho_a(r)^{5/3} - \rho_b(r)^{5/3} \right\} dv \quad (26)$$

with

$$K_k = \frac{3}{5} \frac{\hbar^2 \pi^2}{2m} \left(\frac{3}{\pi}\right)^{2/3} \quad (27)$$

The integration is over the overlap region.

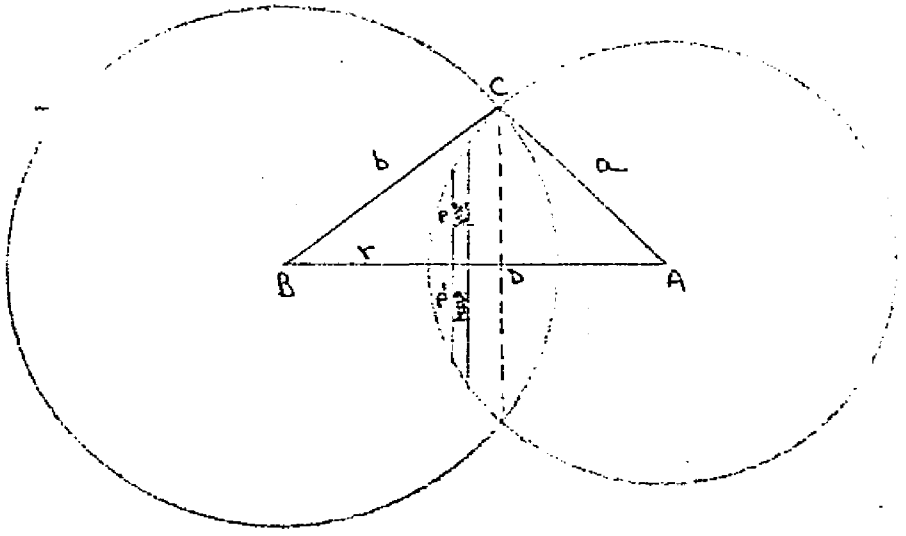

FIGURE 5

The overlap region is divided into two parts by constructing a plane perpendicular to the internuclear axis through CD. By Pythagoras's theorem:

$$AD = \frac{r}{2} + \frac{b^2 - a^2}{2r} \quad (28)$$

$$BD = \frac{r}{2} + \frac{a^2 - b^2}{2r} \quad (29)$$

Consider first the left hand side of the overlap region. A cartesian coordinate system is constructed in the plane of the paper, centered on A, with an s axis along ADB

and a t axis perpendicular to it. Consider an annular ring PP' which has ADB as an axis. p_a and p_b are constant over this ring. The contribution to the kinetic energy from the left part of the overlap region is:

$$E_h^l = 2\pi K_h \int_0^a ds \int_0^g \left[\left\{ p_a(x_1) + p_a(x_2) \right\}^{5/3} - p_a(x_1)^{5/3} - p_b(x_2)^{5/3} \right] t\, dt \qquad (30)$$

with

$$D = \frac{1}{2} r + \frac{a^2 - b^2}{2r} \qquad g = (a^2 - s^2)^{1/2}$$

$$x_1 = (s^2 + t^2)^{1/2} \qquad x_2 = \left[(r-s)^2 + t^2 \right]^{1/2} \qquad (31)$$

The contribution to the kinetic energy is obtained by integrating over a similar coordinate system centered on B:

$$E_h^r = 2\pi K_h \int_0^b ds \int_0^h \left[\left\{ p_a(y_1) + p_b(y_2) \right\}^{5/3} - p_a(y_1)^{5/3} - p_b(y_2)^{5/3} \right] t\, dt \qquad (32)$$

with

$$D = \frac{1}{2} r + \frac{b^2 - a^2}{2r} \qquad g = (b^2 - s^2)^{1/2}$$

$$x_1 = \left[(r-s)^2 + t^2 \right]^{1/2} \qquad x_2 = (s^2 + t^2)^{1/2} \qquad (33)$$

When $r < b-a$ sphere A is inside sphere B. Using the cartesian coordinate system centered on A the kinetic energy is

$$E_h = 2\pi K_h \int_{-a}^a ds \int_0^g \left[\left\{ p_a(x_1) + p_b(x_2) \right\}^{5/3} - p_a(x_1)^{5/3} - p_b(x_2)^{5/3} \right] t\, dt \qquad (34)$$

using the quantities as defined in Eq (31).

For the exchange energy, E_a, the same integrals, Eqs. (30), (32), and (34) are used with the 5/3 powers replaced with 4/3 powers and with K_{AL} replaced by K_a:

$$K_a = \frac{3}{16\pi\epsilon_0}\left(\frac{3}{\pi}\right)^{1/3} e^2 \qquad (35)$$

7. Discussion

The equations were programmed for the Brookhaven CDC 6600 computer. Using the same charge distributions as in Section II we obtain approximate interactions for the same systems in about one-tenth the computer time. The interactions have the same exponential dependence as the quantum mechanical work but they are about 40-50% too low over the region studied. Typical results are shown in Figure 6.

To improve the method a more extensive treatment of exhange effects that arise from the distortion of the electron distributions on overlap to satisfy the exclusion principle is considered. The exchange energy, Eq. (2), is a correction to the electron-electron electrostatic interaction. A correction for the electron-nuclear interaction is sought.

A specific system, Li^+-H^-, will be considered, but the results will be quite general. If $a(r_a)$ and $b(r_b)$ are the one electron wave functions about the Li^+ and H^- respectively, then we can account for exchange effects in LiH by writing the wavefunction as a four by four determinant. The resulting charge distribution taking

exchange effects into account is:

$$\rho(\vec{r}) = -(1+S^2)2a^2(\vec{r}) - (1+S^2)2b^2(\vec{r}) + 4S\,a(\vec{r})\,b(\vec{r}) \qquad (36)$$

where S is the overlap integral

$$S \equiv \langle a | b \rangle \qquad (37)$$

The charge distribution may be considered as being made up of a negative "electronic" charge distribution, ρ_{el}:

$$\rho_{el}(\vec{r}) = -(1+S^2)\left(2a^2(\vec{r}) + 2b^2(\vec{r})\right) \qquad (38)$$

which is the superposition of the free ion charge distributions increased by a factor $(1 + S^2)$, and an "exchange" charge distribution, ρ_{ex}:

$$\rho_{ex} = +4S\,a(\vec{r})\,b(\vec{r}) \qquad (39)$$

which is a positive charge distribution concentrated in the region between the ions. Dick and Overhauser[7] first proposed representing this exchange charge as a point charge of magnitude $+4S^2$ lying on the internuclear axis between the ions. The validity of the approximation has been demonstrated by Hafermeister and Zarht.[8] The validity of this approximation was tested in this study by calculating the dipole moment of LiH using the exact charge distribution and a charge density with a point exchange charge, and the results uphold the validity of the point exchange charge model. The exchange energy is physically equivalent to the interaction between the exchange charge and the electron distributions. In a

similar manner the effects of exchange on the electron-nuclear interaction can be accounted for by considering the interaction between the exchange charge and the nuclei. Since the exchange charge and the nuclei have the same sign of charge this energy will be positive and will increase the interaction energy. In Figure 6 the effect of adding this exchange correction to the interaction calculation is shown. The approximate method now agrees with the diatomic quantum mechanical method to within 10% over the region studied. The inclusion of the exchange-nuclear interaction into the approximate calculations of the $H^- - H$, $H^- - He^o$, and $Li^+ - He^o$ interactions also produced agreement to within 10% of the results of diatomic quantum mechanical calculations of the same systems and over the range studied. The interactions between the host ions and He^o and Li^o were obtained for internuclear separations from 1.6 to 2.4 $\mathring{A}$ in steps of 0.2 $\mathring{A}$. The wave function for the He^o was a screened hydrogenic one with a screening parameter of 1.6875 (z - 5/16). For the Li^o the charge density was taken from the SCF calculations of Herman-Skillman[9]. The interactions were fit to the Born-Mayer form, A exp(-B r) with the parameters given in II.

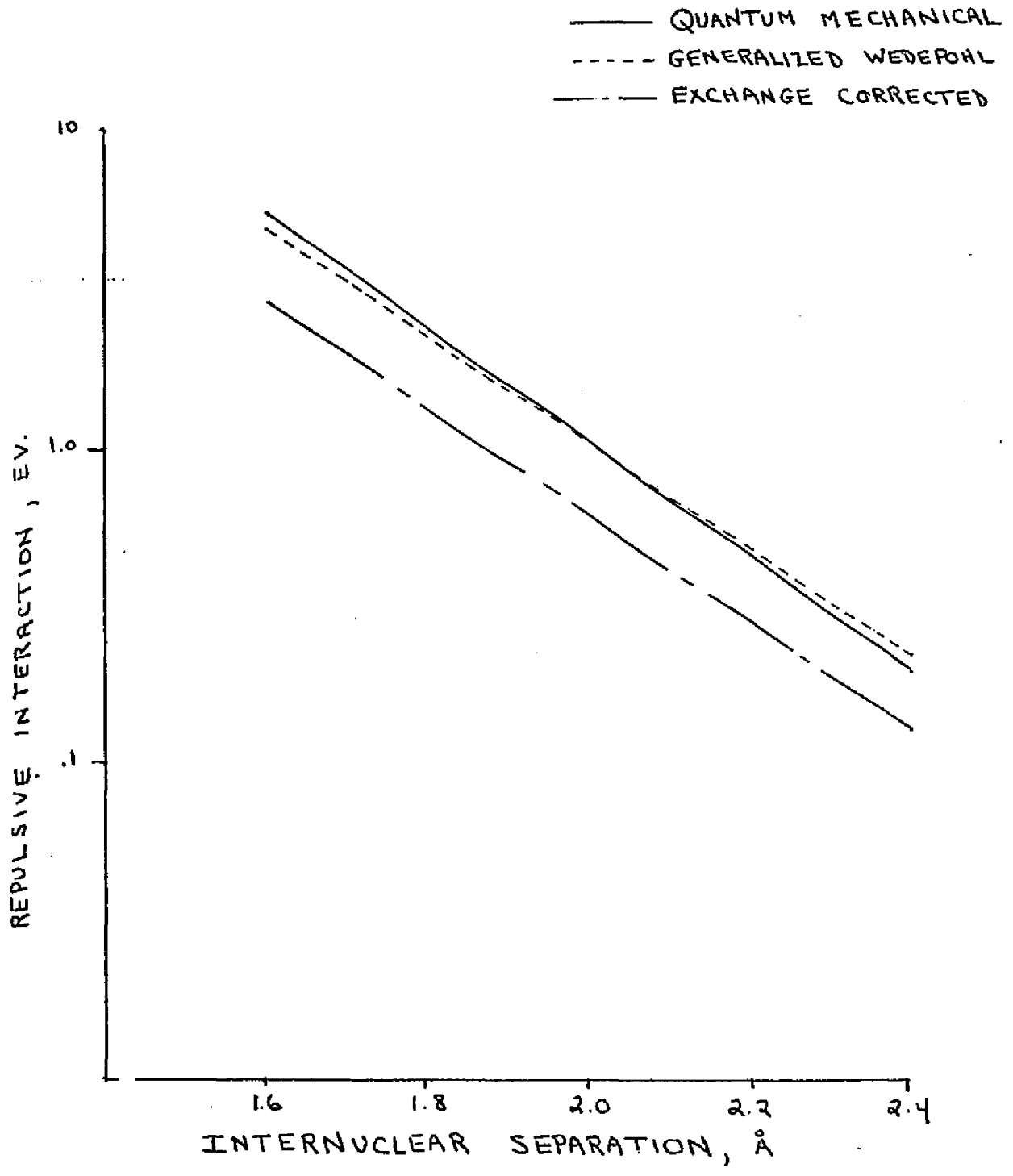
QUANTUM MECHANICAL
GENERALIZED WEDEPOHL
EXCHANGE CORRECTED
10
1.0
.1
REPULSIVE INTERACTION, EV.
1.6
1.8
2.0
2.2
2.4
INTERNUCLEAR SEPARATION, Å

FIGURE 6

References for Appendix I

1. O.B. Firsov, Soviet Physics JETP, 6, 534 (1958).

2. A.A. Abrahamson, R.D. Hatcher, and G. Vineyard, Phys. Rev., 123 538 (1961).

3. A.A. Abrahamson, Phys. Rev., 130, 693 (1963).

4. A.A. Abrahamson, Phys. Rev., to be published.

5. P.T. Wedepohl, Solid St. Commun., 4, 479 (1966).

6. P.T. Wedepohl, Proc. Phys. Soc., 92, 79 (1967).

7. B.G. Dick and A. Overhauser, Phys. Rev., 112, 90 (1958).

8. D.W. Hafemeister and J.D. Zahrt, J. Chem. Phys., 47, 1428 (1967).

9. F. Herman and S. Skillman, Atomic Strucutre Calculations (Prentice Hall, Englewood, New Jersey, 1963).

Appendix II Equivalent Ions Around the Defects

As mentioned in III depending on the symmetry of the defect many ions may have similar displacements and dipoles. For example, if there is a vacancy at (000) then the six ions in the (100) direction are equivalent, the twelve ions in the (110) direction are equivalent, etc. All the defects and host ions are put together into shells. All ions in a shell are equivalent. The number of ions in a shell is called its multiplicity. The coordinates of a typical member of the shell is presented. The parameters which describe the components of the displacement of the typical ion are also listed. The values of the parameters are given for the various defects in Appendix III. To find the displaced position of the typical ion the value of the paramater is added (or if a negative parameter is listed subtracted) from the respective component of its position vector.

Table IX Shells and Displacements Around A Vacancy

Shell	Multiplicity	Typical Ion Position			Displacement Parameters			
		x	y	z	x	y	z	
1	1	0	0	0	0	0	0	Vacancy
2	6	1	0	0	1	0	0	
3	12	1	1	0	2	2	0	
4	8	1	1	1	3	3	3	
5	6	2	0	0	4	0	0	
6	24	2	1	0	5	6	0	

Table X Shells and Displacements Around a Face Center Interstitial

Shell	Multiplicity	Typical Ion Position x	y	z	Displacement Parameters x	y	z	
1	1	0	.5	.5	0	0	0	Interstitial
2	2	0	0	0	0	1	1	
3	2	0	1	0	0	2	-2	
4	4	-1	0	0	3	4	4	
5	4	-1	0	1	5	6	-6	
6	4	0	-1	0	0	7	8	
7	4	0	-1	1	0	9	10	
8	8	-1	-1	1	11	12	13	
9	8	-1	-1	0	14	15	16	
10	4	-2	0	-1	17	18	-18	
11	2	0	-1	1	0	19	-19	
12	4	-2	0	0	20	21	21	
13	2	0	-1	-1	0	22	22	

Table XI Shells and Displacements Around (111) Saddle Point For Host Ion Migration

Shell	Multiplicity	Typical Ion Position			Displacement Parameters			
		x	y	z	x	y	z	
1	2	.2	.2	.2	1	1	1	Interstitials
2	6	1	0	0	2	3	3	
3	6	1	1	0	4	4	5	
4	6	1	0	-1	6	0	-6	
5	2	1	1	1	7	7	7	
6	6	1	1	-1	8	8	9	
7	6	2	0	0	10	11	11	
8	12	2	1	0	12	13	14	
9	12	2	1	-1	15	16	17	

Table XII Shells and Displacements Around (110) Saddle Point for Host Ion Migration

Shell	Multiplicity	Typical Ion Position x	y	z	Displacement Parameters x	y	z	
1	2	.2	.2	0	1	1	0	Interstitials
2	4	1	0	0	2	3	0	
3	2	0	0	1	0	0	4	
4	2	1	1	0	5	5	0	
5	8	1	0	1	6	7	8	
6	2	1	-1	0	9	-9	0	
7	4	1	1	1	10	10	11	
8	4	1	-1	1	12	-12	12	
9	4	2	0	0	13	14	0	
10	2	0	0	2	0	0	15	
11	4	2	1	0	16	17	0	
12	8	2	0	1	18	19	20	
13	4	2	-1	0	21	22	0	

Table XIII Shells and Displacements Around a Divacancy

Shell	Multiplicity	Typical Ion Position			Displacement Parameters			
		X	Y	Z	X	Y	Z	
1	1	0	0	0	0	0	0	Vacancy
2	1	1	0	0	0	0	0	Vacancy
3	4	0	1	0	1	2	0	
4	4	1	1	0	3	4	0	
5	1	-1	0	0	5	0	0	
6	1	2	0	0	6	0	0	
7	4	-1	1	0	7	8	0	
8	4	2	1	0	9	10	0	
9	4	0	1	1	11	12	12	
10	4	1	1	1	13	14	14	
11	4	-1	1	1	15	16	16	
12	4	2	1	1	17	18	18	
13	1	-2	0	0	19	0	0	
14	1	3	0	0	20	0	0	
15	4	0	0	2	21	0	22	
16	4	1	0	2	23	0	24	

Table XIV Shells and Displacements Around a Quadrivacancy

Shell	Multiplicity	Typical Ion Position x	y	z	Displacement Parameters x	y	z	
1	2	0	0	0	0	0	0	Vacancies
2	2	1	0	0	0	0	0	Vacancies
3	4	2	1	0	1	2	0	
4	4	2	0	0	3	4	0	
5	4	1	1	1	5	5	6	
6	4	-1	-1	-1	7	7	8	
7	4	1	0	1	9	-9	10	
8	2	2	2	1	11	11	0	
9	2	2	-1	0	12	-12	0	
10	8	2	0	1	13	14	15	
11	8	2	0	1	16	17	18	
12	4	3	1	0	19	20	0	
13	4	3	0	0	21	22	0	
14	4	1	1	2	23	23	24	
15	4	1	0	2	25	-25	26	

Table XV Shells and Displacements Around a Dinegative Vacancy

Shell	Multiplicity	Typical Ion Position x	y	z	Displacement Parameters x	y	z	
1	2	0	0	0	0	0	0	Vacancies
2	2	1	0	0	1	-1	0	
3	4	2	1	0	2	3	0	
4	4	1	1	1	4	4	5	
5	2	2	2	0	6	6	0	
6	4	2	0	0	7	8	0	
7	4	1	0	1	9	-9	10	
8	8	2	1	1	11	12	13	
9	4	2	2	1	14	14	15	
10	8	2	0	1	16	17	18	
11	4	3	1	0	19	20	0	
12	4	1	1	2	21	21	22	

Table XVI Shells and Displacements Around a Body Center Interstitial

Shell	Multiplicity	Typical Ion Position x	y	z	Displacement Parameters x	y	z	
1	1	.5	.5	.5	0	0	0	Interstitial
2	4	0	0	0	1	1	1	
3	4	0	1	0	2	-2	2	
4	12	-1	0	0	3	4	4	
5	12	-1	0	1	5	6	-6	
6	12	-1	-1	1	7	7	8	
7	12	-1	-1	0	9	9	10	

Appendix III Energy Contributions and Relaxations Around the Defects

Li^+ Body Center Interstitial

Table XVII

Energy Relative to the Perfect Crystal

Electrostatic	-8.1 e.v.
Polarization	-1.7
Repulsive	6.0
Total	-3.8

Displacement Parameters

1	-.15
2	.01
3	.00
4	-.03
5	.01
6	-.05
7	.02
8	.01
9	-.01
10	-.04

Li^+ Face Center Interstitial — Table XVIII

Energy Relative to the Perfect Crystal

Electrostatic	-7.2 e.v.
Polarization	-1.7
Repulsive	5.6
Total	-3.3

Displacement Parameters

1	-.23
2	.04
3	.05
4	-.03
5	-.05
6	-.09
7	-.03
8	-.04
9	-.02
10	.05
11	.00
12	.01
13	.02
14	-.02
15	.02
16	-.04
17	.03
18	.01
19	.01
20	-.03
21	-.02
22	-.04

Li^+ (111) Saddle Point — Table XIX

Energy Relative to the Perfect Crystal

Electrostatic	-7.5 e.v.
Polarization	-1.0
Repulsive	5.1
Total	-3.5

Displacement Parameters

1	.12
2	.01
3	.02
4	.10
5	-.04
6	.01
7	.00
8	.01
9	.01
10	.01
11	-.02
12	-.01
13	.01
14	-.01
15	-.02
16	-.01
17	.01

Li^+ (110) Saddle Point — Table XX

Energy Relative to the Perfect Crystal

Electrostatic	-6.9
Polarization	-1.1
Repulsive	4.7
Total	-3.2

Displacement Parameters

1	.14
2	.07
3	.00
4	-.17
5	.14
6	.05
7	-.04
8	.00
9	.03
10	.00
11	-.02
12	.00
13	.02
14	-.05
15	.08
16	.00
17	.02
18	-.01
19	-.02
20	.00
21	-.02
22	.00

H^- Body Center Interstitial — Table XXI

Energy Relative to the Perfect Crystal

Electrostatic	-7.4 e.v.
Polarization	-3.6
Repulsive	8.6
Total	-2.4

Displacement Parameters

1	-.12
2	-.02
3	.02
4	-.08
5	.00
6	-.02
7	.05
8	.04
9	-.03
10	-.03

H^- Face Center Interstitial — Table XXII

Energy Relative to the Perfect Crystal

Electrostatic	-7.0 e.v.
Polarization	-1.6
Repulsive	7.4
Total	-1.2

Displacement Parameters

1	-.21
2	.09
3	.14
4	-.02
5	-.02
6	-.04
7	-.02
8	-.10
9	-.01
10	.03
11	-.01
12	.04
13	.03
14	-.02
15	-.02
16	-.02
17	-.01
18	.02
19	.05
20	-.03
21	.01
22	-.08

H^- (111) Saddle Point — Table XXIII

Energy Relative to the Perfect Crystal

Electrostatic	-10.3 e.v.
Polarization	-2.4
Repulsive	9.8
Total	-2.9

Displacement Parameters

1	.16
2	.19
3	.02
4	.11
5	-.06
6	.03
7	-.09
8	.03
9	.03
10	.00
11	.00
12	-.03
13	.06
14	.00
15	-.06
16	.00
17	-.02

H^- (110) Saddle Point

Table XXIV

Energy Relative to the Perfect Crystal

Electrostatic	-9.0 e.v.
Polarization	-1.9
Repulsive	8.8
Total	-2.2

Displacement Parameters

1	.17
2	.19
3	.02
4	-.34
5	.13
6	.05
7	.00
8	.02
9	.00
10	.00
11	.00
12	.00
13	.00
14	-.03
15	.04
16	-.03
17	.07
18	-.06
19	.00
20	.03
21	-.04
22	.00

Positive Vacancy

Table XXV

Energy Relative to the Perfect Crystal

Electrostatic	7.5 e.v.
Polarization	-1.4
Repulsive	.2
Total	6.3

Displacement Parameters

1	.07
2	-.01
3	-.01
4	-.05
5	.02
6	.02

Negative Vacancy Table XXVI

Energy Relative to the Perfect Crystal

Electrostatic	5.8 e.v.
Polarization	-.4
Repulsive	-.1
Total	5.3

Displacement Parameters

1	.14
2	-.03
3	-.02
4	.00
5	.03
6	.03

Divacancy

Table XXVII

Energy Relative to the Perfect Crystal

Electrostatic	10.2 e.v.
Polarization	-2.9
Repulsive	1.8
Total	9.0

Displacement Parameters

1	.11
2	.16
3	-.02
4	.06
5	-.18
6	.03
7	-.03
8	-.03
9	.10
10	-.05
11	.02
12	-.04
13	-.07
14	-.03
15	-.07
16	-.03
17	.04
18	-.03
19	-.03
20	-.02
21	-.06
22	-.01
23	.08
24	-.07

Dinegative Vacancy

Table XXVIII

Energy Relative to the Perfect Crystal

Electrostatic	13.7 e.v.
Polarization	- 2.2
Repulsive	2.0
Total	13.2

Displacement Parameters

1	.16
2	.11
3	.07
4	.10
5	.14
6	-.04
7	-.04
8	.02
9	.01
10	-.03
11	-.05
12	.01
13	-.01
14	.03
15	.06
16	-.03
17	-.04
18	.04
19	-.05
20	.01
21	.00
22	-.02

Quadvacancy

Table XXIX

Energy Relative to the Perfect Crystal

Electrostatic	20.8 e.v.
Polarization	-3.6
Repulsive	-.5
Total	16.6

Displacement Parameters

1	.15
2	-.04
3	.02
4	.01
5	-.13
6	.09
7	.11
8	.02
9	-.05
10	.04
11	-.07
12	-.02
13	.07
14	.00
15	-.05
16	-.06
17	-.04
18	-.05
19	.00
20	.01
21	-.03
22	-.05
23	.03
24	-.03
25	.04
26	-.03

Saddle Point for Li^+ Vacancy Migration — Table XXX

Energy Relative to the Perfect Crystal

Electrostatic	6.6 e.v.
Polarization	-2.6
Repulsive	2.2
Total	6.2

Displacement Parameters

1	.06
2	.04
3	-.01
4	-.03
5	.02
6	.00
7	-.01
8	.06
9	-.04
10	.08
11	.04
12	-.05
13	.00
14	.02
15	.01
16	.03
17	.01
18	.03
19	-.06
20	.00
21	.00
22	-.05

Saddle Point for H^- Vacancy Migration — Table XXXI

Energy Relative to the Perfect Crystal

Electrostatic	4.7 e.v.
Polarization	1.6
Repulsive	2.3
Total	5.4

Displacement Parameters

1	.09
2	.14
3	.00
4	-.10
5	.11
6	-.01
7	-.03
8	.00
9	.00
10	.09
11	.00
12	-.02
13	-.04
14	.03
15	.00
16	.05
17	.02
18	.04
19	.00
20	.00
21	.01
22	-.01

He^0 Body Center Interstitial — Table XXXII

Energy Relative to the Perfect Crystal

Electrostatic	-4.1 e.v.
Polarization	-4.0
Repulsive	8.3
Total	.2

Displacement Parameters

1	-.11
2	-.08
3	.01
4	-.03
5	.04
6	-.10
7	-.01
8	.03
9	.03
10	-.05

He^0 Face Center Interstitial — Table XXXII

Energy Relative to the Perfect Crystal

Electrostatic	-3.4 e.v.
Polarization	-1.9
Repulsive	6.1
Total	.8

Displacement Parameters

1	-.17
2	.16
3	.04
4	-.03
5	.03
6	-.11
7	-.01
8	-.03
9	-.01
10	.08
11	-.03
12	.01
13	.02
14	-.02
15	.06
16	-.04
17	-.02
18	.01
19	-.04
20	-.05
21	.02
22	-.02

He^0 on Negative Vacancy

Table XXXIV

Energy Relative to the Perfect Crystal

Electrostatic	5.8 e.v.
Polarization	-.5
Repulsive	.2
Total	5.6

Displacement Parameters

1	.15
2	-.02
3	-.01
4	-.01
5	.02
6	.03

He^0 on Divacancy

Table XXXV

Energy Relative to the Perfect Crystal

Electrostatic	10.2 e.v.
Polarization	- 5.8
Repulsive	1.9
Total	6.3

Displacement Parameters

1	.11
2	.13
3	-.02
4	.06
5	-.17
6	.03
7	-.04
8	-.04
9	.10
10	-.05
11	.02
12	-.04
13	-.07
14	-.03
15	-.07
16	-.03
17	.04
18	-.03
19	-.03
20	-.02
21	-.06
22	-.01
23	.08
24	-.07

He^0 on a Dinegative Vacancy — Table XXXVI

Energy Relative to the Perfect Crystal

Electrostatic	13.5 e.v.
Polarization	-2.3
Repulsive	2.2
Total	13.5

Displacement Parameters

1	.18
2	.10
3	.07
4	.10
5	.14
6	-.06
7	-.04
8	.02
9	.01
10	-.03
11	-.05
12	.01
13	-.01
14	.03
15	.06
16	-.03
17	-.04
18	.04
19	-.05
20	.01
21	.00
22	-.02

He^{O} in Quadvacancy

Table XXXVII

Energy Relative to the Perfect Crystal

Electrostatic	20.8 e.v.
Polarization	- 3.7
Repulsive	- .4
Total	16.7

Displacement Parameters

1	.15
2	-.04
3	.02
4	.01
5	-.13
6	.07
7	.11
8	.02
9	-.05
10	.04
11	-.07
12	-.02
13	.07
14	.00
15	-.05
16	-.06
17	-.04
18	-.05
19	.00
20	.01
21	-.03
22	-.05
23	.03
24	-.03
25	.04
26	-.03

Li^{0} Body Center Interstitial — Table XXXVIII

Energy Relative to the Perfect Crystal

Electrostatic	-5.7 e.v.
Polarization	-4.1
Repulsive	13.6
Total	3.7

Displacement Parameters

1	-.21
2	-.10
3	-.02
4	-.05
5	.04
6	-.09
7	-.03
8	.02
9	-.02
10	-.04

Li^{O} Face Center Interstitial — Table XXXIX

Energy Relative to the Perfect Crystal

Electrostatic	-2.9 e.v.
Polarization	-2.0
Repulsive	9.8
Total	4.9

Displacement Parameters

1	-.26
2	.14
3	.00
4	-.04
5	-.03
6	-.08
7	-.04
8	-.06
9	.02
10	.08
11	-.02
12	-.01
13	.01
14	-.04
15	.03
16	-.03
17	.01
18	.00
19	-.04
20	.03
21	-.01
22	-.05

Li_2^+ on Cation Site Oriented Along (111) Table XI

Energy Relative to the Perfect Crystal

Electrostatic	-3.9 e.v.
Polarization	-2.0
Repulsive	7.2
Total	1.4

Displacement Parameters

1	.06
2	.08
3	-.06
4	.14
5	-.06
6	-.06
7	.00
8	.04
9	.03
10	.00
11	-.10
12	.00
13	.03
14	.00
15	.02
16	-.02
17	-.01

References

1. D.S. Billington, ed., Physics of Solids (Radiation Damage in Solids) (Academic Press, New York, 1963).

2. L.T. Chatterton, Radiation Damage in Crystals (Methuen, London, 1965).

3. F.E. Pretzel, D.T. Vier, E.G. Szklarz, and W.B. Lewis, Radiation Effects on Lithium Hydride, Los Alamos Scientific Report LA-2463 (1961).

4. F.E. Pretzel and R.L. Petty, Phys. Rev., 127, 777 (1962).

5. P.M.S. Jones, The Physical Stability of Metal Tritides. Lithium Tritide and Deuterotritides, United Kingdom Atomic Energy Authority Report, AWRE NO. 0-27/67 (1967).

6. P.C. Souers, T.A. Jolly, and C.F. Cline, J. Chem. Phys.,

7. Y.P. Varshni and R.C. Shulka, Rev. Mod. Phys., 35, 130 (1961).

8. C.R. Fischer, T.A. Dellin, S. Harrison, R.D. Hatcher, and W.D. Wilson to be published.

9. O.L. Anderson, J. Phys. Chem. Solids, 27, 547 (1966).

10 D.R. Stepjens and E.M. Lilley, J. Appl. Phys., 39, 177 (1967)

11. R. Weil and A. W. Lawson, J. Chem. Phys., 37, 2730 (1962).

12. F.E. Voronov, V.A. Goncharova, O.V. Stal'gorova, and T.A. Anipova, Soviet Phys.-Solid State, 8 1313 (1966).

13. P.T. Wedepohl, Proc. Phys. Soc., 92, 79 (1967).

14. C.R. Fischer and P. Kemmey to be published.

15. R.D. Hatcher and G.J. Dienes, Phys. Rev., 134, A214 (1964).

16. National Bureau of Standards, Calculation of Properties of Vacancies and Interstitials (Washington, 1967).

17. J.R. Tessman, A.H. Kahn, and W. Schockley, Phys. Rev., 92, 890 (1953).

18. L. Pauling, Proc. Roy. Soc.(London), A114, 181 (1927).

19. A. Scholz, Phys. Stat. Solidi, 25, 285 (1968).

20. R.J. Quigley and T.P. Das, Solid State Comm., 5 487 (1967).

21. Yamashita and T. Kurosowa, J. Phys. Soc. Japan, 9 944 (1954).

22. L.W. Barr and A.B. Lidiard, Physical Chemistry - An Advanced Treatise, 10, (Academic Press, New York, 1969).

23. C.S. Goldberg to be published.

24. F.C. Brown, The Physics of Solids, (W.A. Benjamin, New York, 1967).

25. K. Tharmilingam, J. Phys. Cem. Solids, 25 255 (1964).

26. J.R. Townsend, Acta Metal., 13, 325 (1965).

26. J.D. Eshelby, "The Continuum Theorey of Lattice Defects in Solid State Physics, 3, ed. by F. Seitz and D. Turnbull (academic Press, New York, 1956)/

28. G.J. Dienes and R. Smoluchowski, J. Phys. Chem. Solids, 27, 611 (1966).